ESAIM: M2AN 47 (2013) 1107–1131
DOI: 10.1051/m2an/2012059

ESAIM: Mathematical Modelling and Numerical Analysis
www.esaim-m2an.org

BOUNDARY CONTROL AND SHAPE OPTIMIZATION FOR THE ROBUST DESIGN OF BYPASS ANASTOMOSES UNDER UNCERTAINTY

Toni Lassila[1], Andrea Manzoni[3], Alfio Quarteroni[1,2] and Gianluigi Rozza[3]

Abstract. We review the optimal design of an arterial bypass graft following either a (i) boundary optimal control approach, or a (ii) shape optimization formulation. The main focus is quantifying and treating the uncertainty in the residual flow when the hosting artery is not completely occluded, for which the worst-case in terms of recirculation effects is inferred to correspond to a strong orifice flow through near-complete occlusion. A worst-case optimal control approach is applied to the steady Navier-Stokes equations in 2D to identify an anastomosis angle and a cuffed shape that are robust with respect to a possible range of residual flows. We also consider a reduced order modelling framework based on reduced basis methods in order to make the robust design problem computationally feasible. The results obtained in 2D are compared with simulations in a 3D geometry but without model reduction or the robust framework.

Mathematics Subject Classification. 35Q93, 49Q10, 76D05.

Received February 1, 2012.
Published online June 17, 2013.

Introduction

Atherosclerosis is a pathology of the arterial system which is driven by the accumulation of fatty materials such as cholesterol in the lumen. As a result the arterial wall first thickens as the plaque grows and in a subsequent stage the lumen narrows, leading to partial or total occlusion. Bypass grafts can provide blood flow through an alternative bridging path in order to overcome critically occluded arteries. One of the most dangerous cases is related to coronary arteries, which supply the oxygen-rich blood perfusion to the heart muscle. The lack of an adequate blood supply may cause tissue ischemia and myocardial infarctions. Coronary artery bypass grafting is a standard surgical procedure to restore blood perfusion to the cardiac muscle by redirecting blood from the Aorta through a graft vessel (either artificial or biological) to the downstream of the occluded coronary artery. The design of the end-to-side anastomosis that connects the graft vessel to the host

Keywords and phrases. Optimal control, shape optimization, arterial bypass grafts, uncertainty, worst-case design, reduced order modelling, Navier-Stokes equations.

[1] Modelling and Scientific Computing, Mathematics Institute of Computational Science and Engineering, École Polytechnique Fédérale de Lausanne, Station 8, EPFL, 1015 Lausanne, Switzerland. toni.lassila@epfl.ch; alfio.quarteroni@epfl.ch

[2] MOX, Modellistica e Calcolo Scientifico, Dipartimento di Matematica F. Brioschi, Politecnico di Milano, Piazza Leonardo da Vinci 32, 20133 Milano, Italy. alfio.quarteroni@polimi.it

[3] Now at SISSA MathLab, International School for Advanced Studies, Via Bonomea 265, 34136 Trieste, Italy. andrea.manzoni@sissa.it; gianluigi.rozza@sissa.it

Article published by EDP Sciences

© EDP Sciences, SMAI 2013

https://doi.org/10.1051/m2an/2012059 Published online by Cambridge University Press

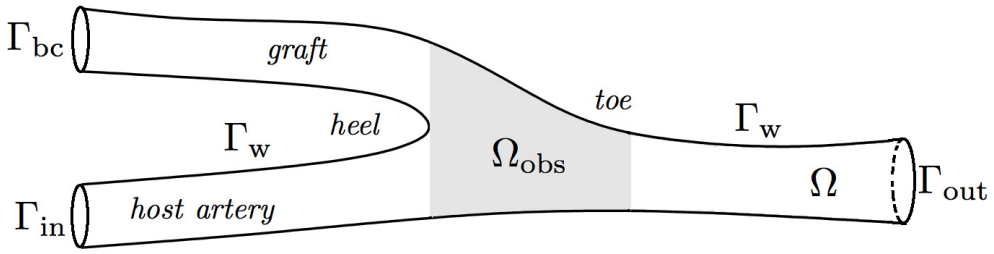


FIGURE 1. A schematic view of a bypass graft anastomosis.

vessel is a critical factor in avoiding post-operative recurrence of the stenosis, since fluid dynamic phenomena such as recirculation, oscillating or untypically high/low shear rates, and stagnation areas can cause the growth of another stenosis downstream from the anastomosis. Different kinds and shapes for aorto-coronaric bypass anastomoses are available, such as Miller cuffed models or Taylor patches [25, 39]. The connection of the graft to the coronary artery can be done using an end-to-side or a side-to-side anastomosis; a detailed survey of the predominant flow features of end-to-side anastomoses is provided in [39].

The major factors known to strongly influence the recurrence of intimal hyperplasia are related to low or oscillating Wall Shear Stress (WSS) [32,33] occurring near the anastomosis. Hence, a typical attempt to design a bypass graft is apt at minimizing some cost functionals related to haemodynamic quantities. Numerical methods of Computational Fluid Dynamics (CFD) can help in understanding local haemodynamics phenomena and the effect of vascular wall modification on flow patterns (see *e.g.* [39]). On the other hand, theoretical methods of optimal control and shape optimization enable a suitable formulation of the optimal design problem for bypass grafts. Many works [1, 2, 16, 17, 21, 35, 38, 43, 49, 51, 56, 58] have focused in the last decade on the optimal shape design of end-to-side anastomoses, typically by acting on the wall shape near the anastomosis by local shape variations. The three most significant design variables in end-to-side anastomoses are [39]: the anastomosis angle, the graft-to-host diameter ratio [32], and the toe shape (see Fig. 1). Also the flow split between the proximal host artery and the graft affects greatly the distribution of WSS [21], as do the viscosity and the Reynolds number. The effect of the flow profile at or near the inlets must also be taken into account. The near-complete occlusion of stenotic arteries produces the largest (often turbulent) disturbances in the flow, and has been linked to triggering biochemical processes such as thrombosis, hemolysis etc. While it is known that the physical unsteady and pulsatile flow can be replaced with a steady mean flow with the same Reynolds number for purposes of evaluating the mean WSS distribution[4], the correct flow profile must be taken into account if accurate WSS predictions are desired[5]. It seems clear that in order to design a bypass graft in a robust way, one must be prepared to take into account all the various sources of *uncertainty* that can effect the final optimized design. Concerning previous works on optimization of bypass anatomoses, the effect of the anastomosis angle was studied in [16, 17, 37, 58], the effect of the toe shape in [1, 2, 18, 37, 38, 43, 56], and the graft-to-host ratio in [16]. For a more complete review of bypass graft design results, we refer to [45, 47].

Only recently the effect of uncertainty in the design of bypass grafts has been taken into account. In [58] the bypass configuration was optimized under unsteady flow with an uncertain flow split between the occluded artery and the graft. The robust design was sought by minimizing a cost functional that measured the area of low wall shear stress in the downstream region of the anastomosis. To make the design robust, the authors

[4] Both steady and unsteady flow cases in a bypass anastomosis were studied in [40, 41] and, assuming the same mean Reynolds number, both types of flows were found to produce similar mean WSS distributions. In [20] the steady flow case was proposed as a reference that can be used to separate the effects of the anastomosis geometry and the flow pulsatility on the WSS.

[5] For example, in [63] the effect of cardiac motion on the flow in a coronary artery was studied: it was shown that the motion-induced change in the velocity profile could impact the WSS values by up to 150%.

https://doi.org/10.1051/m2an/2012059 Published online by Cambridge University Press

added a penalty term for the standard deviation of the output due to input uncertainties. The cost of such an optimization method was reported as quite high, 11 days in the fully 3D unsteady case on a 18×4 cores parallel cluster. In [35] a similar problem was considered for steady 2D flow, but optimizing the whole shape rather than just the angle. The computational cost was diminished by introducing a Reduced Order Model (ROM) for the fluid equation based on Reduced Basis (RB) methods, making the robust design problem computationally feasible. In [49] the bypass shape was obtained by minimizing the total shear rate, and the sensitivity of the optimal shape with respect to the uncertain viscosity in a non-Newtonian rheology was considered. There was no attempt made to find a robust optimal shape over a range of viscosity values, likely due to prohibitive cost of running the full-fidelity three-dimensional finite element simulations. These preliminary works already indicate that in presence of uncertainty effects the bypass design problem is not yet satisfactorily solved by existing classical computational approaches, and, furthermore, that some type of ROM is needed to reduce the computational cost.

The goal of this work is to provide a wide theoretical and numerical framework to deal with optimal design problems related to bypass anastomoses. In particular, both an optimal control and a shape optimization formulation are provided. Moreover, a new contribution of this work is aimed at inserting some uncertainty elements (featuring the nature of the residual flow in the partially occluded arterial branch) in both these problems. The main novelty is in using a min-max formulation for solving the optimal design problem under uncertainty. For the numerical solution of both optimal control and shape optimization problems, we exploit some recent developments we achieved in the Reduced Basis methodology for parametrized PDEs, which allow a remarkable – and necessary – reduction of computational costs and geometrical complexity, whenever interested in the optimization of the bypass anastomosis shape.

Previous works on model reduction of shape optimization/optimal control problems have often applied the Proper Orthogonal Decomposition (POD) on a collection of snapshot solutions to produce a low-dimensional basis for a ROM that is suitable for approximating the nonlinear PDE system. The two main challenges are: (i) how to guarantee that the approximation is sufficiently accurate at the parameter values that were not included in the original snapshot set, and (ii) how to verify that the optimal design given by the ROM is also optimal for the full-order problem? Many techniques have been proposed specifically for extending the validity of POD bases in the parametric optimization context, *e.g.* by adaptive resampling of the parameter space, by enhancing the POD basis with parametric sensitivity snapshots [10, 62], by interpolating between ROMs computed at different snapshot locations [4], or by using trust-region methods to gauge if an existing ROM is sufficiently accurate or whether it should be refined [7]. In contrast our RB method is trained using the greedy-in-parameter algorithm, which theoretically will produce a uniformly accurate ROM. A completely different approach was recently proposed in [5], where a domain-decomposition-inspired method was based on a localized full-order model evaluated around the shape to be designed and coupled to a ROM for the "far-field", which had no explicit dependence on the design parameters. The second issue is how to avoid suboptimal designs based on the ROM. If the cost function is a linear (or quadratic) function of the state, the error in the optimality system can be estimated by constructing another ROM for a dual problem (see *e.g.* [5, 46]). Other options include successive refinement of the ROM using full-order solutions computed at each sub-optimal design configuration [54], and the use of trust-region methods [7]. We do not address the suboptimality question in this work.

The structure of the paper is as follows. We review some features related to the optimal design of bypass grafts (Sect. 1) and present two different paradigms based on optimal control and shape optimization, highlighting key points and difficulties. In the first case, a simplified 2D boundary control formulation is considered (Sect. 2), incorporating uncertainty about residual flows through the stenosed artery. In the second case, a 2D shape optimization problem is considered (Sect. 3), dealing with robust design under uncertainty. For the sake of computational saving, these problems are solved within a suitable ROM framework, presented in Section 4. Numerical results, as well as a comparison with simplified 3D configurations, are detailed in Section 5–6, followed by some conclusions in Section 7.

https://doi.org/10.1051/m2an/2012059 Published online by Cambridge University Press

1. Mathematical modelling for bypass optimal design

Haemodynamic factors like flow recirculation or stagnation, as well as high vorticity or dissipation regions, low and oscillatory WSS, may play a driving role in the development of vascular diseases under certain assumptions [21,33,37,39]. Hence, meaningful mathematical models and description of blood flows, together with accurate numerical simulations, can have useful clinical applications especially in surgical procedures. However, a rigorous model for blood circulation should take into account (i) the flow unsteadiness, (ii) the arterial wall deformability, described by suitable structural models [29] and possibly (iii) complex rheological model to characterize the aggregate nature of the blood [55]. In view of studying optimal control and shape optimization problems, which entail the repeated simulation of these flow equations (and the evaluation of the cost functional to be minimized), we cannot afford the solution of PDE models involving such complex features – computational costs would be too prohibitive[6]. For these reasons, we model blood flows adopting steady incompressible Navier-Stokes equations for laminar Newtonian flow with the velocity field $\mathbf{v}$ and pressure field p satisfying

$$\begin{cases} -\nu\Delta\mathbf{v} + (\mathbf{v}\cdot\nabla)\mathbf{v} + \frac{1}{\rho}\nabla\mathbf{p} = \frac{1}{\rho}\mathbf{f} & \text{in} \quad \Omega \\ \nabla\cdot\mathbf{v} = \mathbf{0} & \text{in} \quad \Omega \\ \mathbf{v} = (Q_{\text{tot}} - Q_{\text{in}}(\mathbf{u}_{\text{in}}))\mathbf{u}_{\text{bc}} & \text{on} \quad \Gamma_{\text{bc}} \\ \mathbf{v} = \mathbf{u}_{\text{in}} & \text{on} \quad \Gamma_{\text{in}} \\ \mathbf{v} = \mathbf{0} & \text{on} \quad \Gamma_w \\ -p\mathbf{n} + \nu\dfrac{\partial\mathbf{v}}{\partial\mathbf{n}} = \mathbf{0} & \text{on} \quad \Gamma_{\text{out}}. \end{cases} \tag{1.1}$$

Here $\Omega \subset \mathbb{R}^d$ for $d = 2, 3$ is assumed to be piecewise C^2 with convex corners, representing an end-to-side anastomosis (see Fig. 1). The Dirichlet portion Γ_D of the boundary is further divided into the inlet from the stenosed section of the artery Γ_{in} and the bypass inlet Γ_{bc}, where we prescribe two inflow profiles $\mathbf{u}_{\text{in}}$ and $\mathbf{u}_{\text{bc}}$ respectively, and the walls, where we prescribe a no-slip boundary condition. We assume a "do-nothing" boundary condition at the outlet $\Gamma_{\text{out}} \neq \emptyset$. Moreover, blood dynamic viscosity is $\mu = 0.04\ \text{g}\,\text{cm}^{-1}\,\text{s}^{-1}$, blood density $\rho = 1\ \text{g}\,\text{cm}^{-3}$, thus yielding a kinematic viscosity $\nu = \mu/\rho = 0.04\ \text{cm}^2\,\text{s}^{-1}$ and a Reynolds number $Re = \tilde{v}D/\nu$ of order 100. The corresponding weak form of Navier-Stokes equations (1.1) reads: find $(\mathbf{v}, p, \boldsymbol{\eta}) \in \mathcal{Y}\times\mathcal{Q}\times\mathcal{G}$ s.t.

$$\mathcal{A}(\mathbf{v}, p, \boldsymbol{\eta}; \mathbf{z}, q, \boldsymbol{\lambda}) := a(\mathbf{v}, \mathbf{z}) + b(p, \mathbf{z}) + b(q, \mathbf{v}) + c(\mathbf{v}, \mathbf{v}, \mathbf{z}) + g_D(\mathbf{z}, \boldsymbol{\eta}) + g_D(\mathbf{u} - \mathbf{u}_D, \boldsymbol{\lambda}) \ = \ 0, \tag{1.2}$$

for all $(\mathbf{z}, q, \boldsymbol{\lambda}) \in \mathcal{Y}\times\mathcal{Q}\times\mathcal{G}$, where the continuous bilinear and trilinear forms are defined as

$$a(\mathbf{v}, \mathbf{z}) := \nu\int_\Omega \nabla\mathbf{u} : \nabla\mathbf{z}\,\mathrm{d}\Omega, \quad b(p, \mathbf{z}) := -\frac{1}{\rho}\int_\Omega p\ \text{div}\ \mathbf{z}\,\mathrm{d}\Omega, \quad c(\mathbf{v}, \mathbf{w}, \mathbf{z}) := \int_\Omega (\mathbf{v}\cdot\nabla)\mathbf{w}\cdot\mathbf{z}\,\mathrm{d}\Omega,$$

and the duality pairing $g_D : (H^{1/2}(\Gamma_D))^d \times (H^{-1/2}(\Gamma_D))^d \to \mathbb{R}$ is used to enforce a Dirichlet boundary condition on $\Gamma_{\text{in}} \cup \Gamma_{\text{w}} \cup \Gamma_{\text{bc}} =: \Gamma_D \subset \partial\Omega$ with boundary data $\mathbf{u}_D$. The velocity space is chosen as $\mathcal{Y} := [H^1(\Omega)]^d$, the pressure space as $\mathcal{Q} := L^2(\Omega)$, and the Lagrange multiplier space

$$\mathcal{G} := [H^{-1/2}(\Gamma_D)]^d.$$

We denote $\mathbf{L}_{\text{bc}}, \mathbf{L}_{\text{in}} \in \mathcal{Y}$ two divergence-free lifting functions of the boundary data $\mathbf{u}_{\text{bc}}$ and $\mathbf{u}_{\text{in}}$, such that $\mathbf{L}_{\text{bc}}|_{\Gamma_{\text{bc}}} = \mathbf{u}_{\text{bc}}$ and $\mathbf{L}_{\text{in}}|_{\Gamma_{\text{in}}} = \mathbf{u}_{\text{in}}$ on Γ_{bc} and Γ_{in}, respectively. Moreover, in order to have a physically meaningful problem, we enforce the total conservation of fluxes between the (partially or totally) occluded branch Γ_{in} and the graft inlet Γ_{bc}, according to

$$\begin{aligned} Q_{\text{in}}(\mathbf{v}_{\text{in}}) \ &:= \ \int_{\Gamma_{\text{in}}} \mathbf{v}_{\text{in}}\cdot\mathbf{n}\,\mathrm{d}\Gamma, \quad \int_{\Gamma_{\text{bc}}} \mathbf{v}_{\text{bc}}\cdot\mathbf{n}\,\mathrm{d}\Gamma \equiv 1, \\ Q_{\text{tot}} \ &= \ Q_{\text{in}}(\mathbf{v}_{\text{in}}) + (Q_{\text{tot}} - Q_{\text{in}}(\mathbf{v}_{\text{in}}))\int_{\Gamma_{\text{bc}}} \mathbf{v}_{\text{bc}}\cdot\mathbf{n}\,\mathrm{d}\Gamma, \end{aligned} \tag{1.3}$$

where Q_{tot} is the known and constant flow rate in the host artery before the bypass.

[6] In the steady case we take into account the peak flowrate at the inlet.

https://doi.org/10.1051/m2an/2012059 Published online by Cambridge University Press

To show the well-posedness of the inhomogeneous Navier-Stokes equations (1.2), we cite a classical stability and uniqueness result under the assumption of *small data* (for the proof, see *e.g.* [60], Chap. 2, Thm. 1.6):

Lemma 1.1. *Assume that* $\mathbf{u}_{\rm in} \in [H^{1/2}(\Gamma_{\rm in})]^d$, $\mathbf{u}_{\rm bc} \in [H^{1/2}(\Gamma_{\rm bc})]^d$ *and* Ω *is of class* C^2. *The velocity field* $\mathbf{v} \in \mathcal{Y}$ *defined as the solution of* (1.2) *satisfies the stability estimate*

$$\|\mathbf{v}\|_1 \leq \frac{2}{\nu}\|\widetilde{f}(\mathbf{L}_{\rm in}, \mathbf{L}_{\rm bc})\|_{-1},$$

where

$$\|\widetilde{f}(\mathbf{L}_{\rm in}, \mathbf{L}_{\rm bc})\|_{-1} := \sqrt{\left\|\nu\triangle\mathbf{L}_{\rm in} - \sum_{i=1}^{d}[\mathbf{L}_{\rm in}]_i\partial_{x_i}\mathbf{L}_{\rm in}\right\|^2_{H^{-1}(\Omega)} + \left\|\nu\triangle\mathbf{L}_{\rm bc} - \sum_{i=1}^{d}[\mathbf{L}_{\rm bc}]_i\partial_{x_i}\mathbf{L}_{\rm bc}\right\|^2_{H^{-1}(\Omega)}}.$$

In addition, provided that

$$|c(\mathbf{w}, \mathbf{L}_{\rm in}, \mathbf{w})| + |c(\mathbf{w}, \mathbf{L}_{\rm bc}, \mathbf{w})| \leq \frac{\nu}{2}\|\mathbf{w}\|_1^2 \quad \textit{for all } \mathbf{w} \in \mathcal{Y} \tag{1.4}$$

and[7]

$$\nu^2 > 4\, C_d\, \|\widetilde{f}(\mathbf{L}_{\rm in}, \mathbf{L}_{\rm bc})\|_{-1}, \tag{1.5}$$

where $C_d > 0$ *is the Sobolev embedding constant s.t.* $|c(\mathbf{v}, \mathbf{w}, \mathbf{z})| \leq C_d\|\mathbf{v}\|_1\|\mathbf{w}\|_1\|\mathbf{z}\|_1$ *for all* $\mathbf{v}, \mathbf{w}, \mathbf{z} \in \mathcal{Y}$, *then the solution* $\mathbf{v}$ *is unique and depends continuously on the boundary data* $(\mathbf{u}_{\rm in}, \mathbf{u}_{\rm bc})$.

To pose the optimal design problem, several cost functionals depending on the state solution $(\mathbf{v}, p)$ have been proposed in literature for the optimization of arterial bypass grafts or otherwise regularization of flows where recirculation and vortex generation are to be minimized. By denoting $\Omega_{\rm obs}$ the subdomain where physical indices of interest are observed, we list some typical choices together with references to previous works where such functionals have been employed:

1. *viscous energy dissipation* [35, 49]

$$J_1(\mathbf{v}) := \frac{\nu}{2}\int_{\Omega_{\rm obs}} |\nabla\mathbf{v}|^2\, \mathrm{d}\Omega \quad \text{or} \quad J_1(\mathbf{v}) := \frac{\nu}{2}\int_{\Omega_{\rm obs}} \varepsilon(\mathbf{v}) : \varepsilon(\mathbf{v})\, \mathrm{d}\Omega,$$

   being $\varepsilon(\mathbf{v}) = (\nabla\mathbf{v} + \nabla\mathbf{v}^T)/2$ the Cauchy strain tensor;

2. *Stokes-tracking type functional* [28, 31, 35]

$$J_2(\mathbf{v}) := \int_{\Omega_{\rm obs}} |\mathbf{v} - \mathbf{v}_{\rm Stokes}|^2\, \mathrm{d}\Omega,$$

   where $\mathbf{v}_{\rm Stokes}$ is the solution of (1) obtained after neglecting the term $c(\mathbf{v}, \mathbf{v}, \mathbf{z})$;

3. *vorticity* [2, 6, 31, 35, 56]

$$J_3(\mathbf{v}) := \frac{\nu}{2}\int_{\Omega_{\rm obs}} |\nabla\times\mathbf{v}|^2\, \mathrm{d}\Omega,$$

[7] This condition is far from being guaranteed in realistic flows, however, it is standard in works on optimal control of Navier-Stokes equations [24].

https://doi.org/10.1051/m2an/2012059 Published online by Cambridge University Press

4. *Galilean invariant* vortex measure for two-dimensional flows [28,31,35]

$$J_4(\mathbf{v}) := \int_{\Omega_{\text{obs}}} \max\{\det(\nabla \mathbf{v}), 0\}\, \mathrm{d}\Omega \quad \text{or} \quad J_4(\mathbf{v}) := \int_{\Omega_{\text{obs}}} g(\det(\nabla \mathbf{v}))\, \mathrm{d}\Omega,$$

where $g(z)$ is a smooth nonnegative function satisfying $g(z) = 0$ for $z \leq 0$ and $g(z) = \mathcal{O}(z)$ as $z \to \infty$ [31]. This choice is motivated by the fact that vortex cores are related to regions where the eigenvalues of $\nabla \mathbf{v}$ are complex, and in the two-dimensional case this is equivalent to $\det(\nabla \mathbf{v}) > 0$.

5. *wall shear stress gradient* (WSSG) [37,50]

$$J_5(\mathbf{v}) := \int_{\Gamma_{\text{obs}}} \left(\left| \frac{\partial \tau_w}{\partial \xi_a} \right|^2 + \left| \frac{\partial \tau_w}{\partial \xi_c} \right|^2 \right) \mathrm{d}\Gamma$$

where τ_w denotes the wall shear stress vector, and ξ_a, ξ_c the tangent vectors in the axial and circumferential directions respectively. It is known that the time-averaged WSS can be relatively insensitive to changes in the anastomosis configuration, but that the time-averaged WSS gradient is highly sensitive and has been linked to localized mechanobiological responses in tissues (see [37] and discussion therein). This can be understood as filtering the WSS by removing its component induced by the steady mean flow and considering only the spatially fluctuating term as part of the indicator. To this end we adopt in this work the WSS gradient of the steady flow as an approximation of the time-averaged WSS gradient.

The functionals J_1–J_4 are all bounded in $[H^1(\Omega)]^d$. The energy functionals J_1 are analytically the simplest to handle. They are coercive and weakly coercive owing to the Poincaré and Korn inequalities respectively[8]. The tracking functional J_2 is suitable only for low-Reynolds flows with negligible convective effects. The vorticity functional J_3 is the most common choice, but it has the problem that strong shear boundary layers can have a disproportionate weight compared to the vortices. The functional J_4 is not differentiable and needs to be regularized to make it regular enough to use the standard optimal control framework.

The WSSG functional J_5 is very difficult to treat in a rigorous mathematical way, since even with added regularity for the solution, say $(\mathbf{v}, q) \in [H^{s+1}(\Omega)]^d \times H^s(\Omega)$ for some $s \geq 1$, one is only able to obtain $\tau_w \in [H^{s-3/2}(\Gamma)]^d$ and *a priori* the tangential derivatives of WSS might not exist even in a weak sense unless $s \geq 3$. Such a result requires the unrealistic assumptions of the domain being of class $\mathcal{C}^{s+1}$, and the inhomogeneous boundary data being in $[H^{s-1/2}(\Gamma)]^d$ (see *e.g.* [60], Chap. 2, Prop. 1.1). Even if sufficient regularity can theoretically be achieved, if a computational approximation for the velocity needs to be sought in a subspace of the Sobolev space $[H^4(\Omega)]^d$, the use of spectral methods or isogeometric analysis with highly regular basis functions may be necessary to recover sufficiently smooth WSS values. Based on these considerations, we concentrate in the numerical examples on three cost functionals: the viscous energy dissipation J_1, the vorticity J_3, and the vortex measure J_4.

The observation region Ω_{obs} should be chosen so that it focuses on the regions where restenosis and intimal hyperplasia is known to occur post-treatment. Typically this involves the region around the heel and the toe, but can also include the bottom wall of the host artery extending further into the distal branch. Depending on the functional chosen we may have to limit ourselves to considering only effects near the anastomosis exit. This is especially important when using the vorticity functional J_3, as it is known that strong shear flow along the arterial walls can mask the vortices [30]. In this case the total length of the observation domain should be as small as possible to avoid such issues. In Figure 1 we sketch a typical observation region Ω_{obs}. When using WSS functionals one has to operate on wall quantities, and so one can choose for example $\Gamma_{\text{obs}} := \overline{\Omega}_{\text{obs}} \cap \Gamma_w$.

[8] Coercivity holds at least if $\Omega_{\text{obs}} = \Omega$. If $\Omega_{\text{obs}} \subsetneq \Omega$, as is usually the case in practice as we want to focus the reduction to a subregion near the anastomosis, we do not have analytical results but typically the convexity and coercivity of the cost functional is preserved as we shall see in the results section.

https://doi.org/10.1051/m2an/2012059 Published online by Cambridge University Press

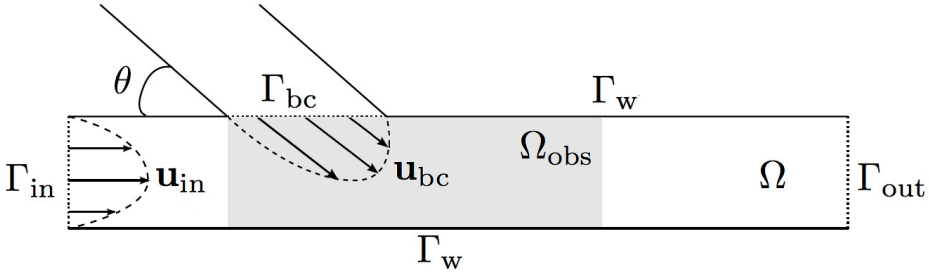


FIGURE 2. Domain and boundary segments for the optimal boundary control formulation.

2. A BOUNDARY OPTIMAL CONTROL FORMULATION FOR BYPASS DESIGN

2.1. Formulation of a robust design problem as a min-max problem

A first possible approach for the optimal design of bypass grafts is based on the solution of a suitable optimal control (OC) problem in the vein of [6, 12, 23, 28, 34], for which the control function is the Dirichlet boundary condition representing the flow entering into the artery from the graft on the boundary[9] $\Gamma_{\rm bc}$. Thus the geometrical properties of the bypass graft are only represented by the velocity profile $\mathbf{u}_{\rm bc} \in \mathcal{U}_{\rm bc}$ imposed at the bypass anastomosis, which has to be controlled in order to minimize a given cost functional. This entails the solution of a problem on a *frozen*, fixed domain – the one given by the occluded artery – on which the state Navier-Stokes equations (now representing a constraint), have to be solved. For simplicity we refer also to problems following this formulation as design problems, even if they only involve boundary control.

If the residual flow function $\mathbf{u}_{\rm in}$ through the occluded section $\Gamma_{\rm in}$ is known, the *deterministic design (OC) problem* can be formulated as follows: given $\mathbf{u}_{\rm in}$, find the boundary control function $\mathbf{u}_{\rm bc}$ solving

$$\min_{\mathbf{u}_{\rm bc}\in\mathcal{U}_{\rm bc}} J(\mathbf{v};\mathbf{u}_{\rm bc},\mathbf{u}_{\rm in}) \quad \text{s.t.} \quad \mathcal{A}(\mathbf{v},p,\boldsymbol{\eta};\mathbf{z},q,\boldsymbol{\lambda};\mathbf{u}_{\rm bc},\mathbf{u}_{\rm in})=0, \quad \forall\,(\mathbf{z},q,\boldsymbol{\lambda})\in\mathcal{Y}\times\mathcal{Q}\times\mathcal{G}, \tag{DD-OC}$$

where $J:\mathcal{Y}\to\mathbb{R}_0^+$ is a cost functional measuring the graft performance (e.g. one of the functionals listed in Sect. 1) and $\mathcal{A}(\cdot;\cdot;\mathbf{u}_{\rm bc})$ is the Navier-Stokes operator defined in (1.2). Here the dependence of the state equation and the cost functional on the control variable $\mathbf{u}_{\rm bc}$ and the residual flow $\mathbf{u}_{\rm in}$ has been highlighted.

On the other hand, assuming that the patency of the occluded artery (and the corresponding residual flow $\mathbf{u}_{\rm in}$) is uncertain, we consider the following worst-case design problem:

> *Find the bypass control function* $\mathbf{u}_{\rm bc}$ *in such a way that it minimizes the worst-case value of* $J(\mathbf{v})$ *over all admissible values of the residual flow function* $\mathbf{u}_{\rm in}$.

To obtain a satisfactory answer to this problem, we study the so-called *robust design problem*: find the boundary control function $\mathbf{u}_{\rm bc}$ solving the worst-case optimization problem

$$\min_{\mathbf{u}_{\rm bc}\in\mathcal{U}_{\rm bc}} \max_{\mathbf{u}_{\rm in}\in\mathcal{U}_{\rm in}} J(\mathbf{v};\mathbf{u}_{\rm bc},\mathbf{u}_{\rm in}) \quad \text{s.t.} \quad \mathcal{A}(\mathbf{v},p,\boldsymbol{\eta};\mathbf{z},q,\boldsymbol{\lambda};\mathbf{u}_{\rm bc},\mathbf{u}_{\rm in})=0, \quad \forall\,(\mathbf{z},q,\lambda)\in\mathcal{Y}\times\mathcal{Q}\times\mathcal{G}. \tag{RD-OC}$$

The robust design problem can be understood as a one-shot game, where the designer of the bypass plays first and chooses the control function $\mathbf{u}_{\rm bc}$ to minimize the cost functional J. The second player then follows by choosing the residual flow function $\mathbf{u}_{\rm in}$ to maximize the cost function J. The payoff for the designer is $-J$ and for the second player J. Thus the optimal strategy for the designer is given as the solution of a min-max type of strategy obtained by solving (RD-OC), while the second player will choose his response by solving another

[9] With respect to the general case of Section 1, here $\Gamma_{\rm bc}$ is a (fictitious) boundary representing the anastomosis (see Fig. 2).

https://doi.org/10.1051/m2an/2012059 Published online by Cambridge University Press

problem. We call this the *complementary uncertainty problem* and it is defined as: given a known boundary control function $\mathbf{u}_{\mathrm{bc}}$, find the residual flow function $\mathbf{u}_{\mathrm{in}}$ maximizing the cost functional

$$\max_{\mathbf{u}_{\mathrm{in}}\in\mathcal{U}_{\mathrm{in}}} J(\mathbf{v};\mathbf{u}_{\mathrm{bc}},\mathbf{u}_{\mathrm{in}}) \quad \text{s.t.} \quad \mathcal{A}(\mathbf{v},p,\boldsymbol{\eta};\mathbf{z},q,\boldsymbol{\lambda};\mathbf{u}_{\mathrm{bc}},\mathbf{u}_{\mathrm{in}})=0, \quad \forall\,(\mathbf{z},q,\lambda)\in\mathcal{Y}\times\mathcal{Q}\times\mathcal{G}. \tag{CU}$$

Concerning the well-posedness of these problems, a general existence result for the first optimality problem (DD-OC) can be found in [23] (see Lem. 2.1 and the related proof):

Theorem 2.1. *Assume that the cost functional* $J(\mathbf{v})$

(*i*) *is bounded,* i.e. *there exists* $C_0>0$ *s.t.* $J(\mathbf{v})\le C_0\|\mathbf{v}\|_1^2$*;*
(*ii*) *is convex,* i.e. *for any* $\mathbf{u}_1,\mathbf{u}_2\in[H^1(\Omega)]^d$ *and* $\gamma\in[0,1]$ *it holds that* $(1-\gamma)J(\mathbf{u})+\gamma J(\mathbf{u})\ge J((1-\gamma)\mathbf{u}+\gamma\mathbf{u})$*;*
(*iii*) *satisfies for some constants* $C_1,C_2,C_3>0$ *the weak coercivity inequality*

$$J(\mathbf{v})\ge C_1\|\mathbf{v}\|_1^2-C_2\|\mathbf{v}\|_1-C_3 \quad \text{for all } \mathbf{v}\in\mathcal{Y}. \tag{2.1}$$

Let the admissible set $\mathcal{U}_{\mathrm{bc}}$ *for the control function be a closed and convex subset of* $[H^{1/2}(\Gamma_{\mathrm{bc}})]^d$*. Then the problem* (DD-OC) *admits at least one optimal solution.*

The well posedness of the third problem (CU) is ensured by the following result:

Theorem 2.2. *Assume that* Γ_{in} *is an open and connected subset of* $\partial\Omega$*, and that the cost functional* $J(\mathbf{v})$

(*i*) *is bounded (see (i), Thm. 2.1);*
(*ii*) *is upper semicontinuous,* i.e. $\limsup_{\mathbf{v}\to\mathbf{v}^*} J(\mathbf{v})\le J(\mathbf{v}^*)$ *for all* $\mathbf{v}^*\in\mathcal{Y}$.

Let the admissible set $\mathcal{U}_{\mathrm{in}}\subseteq\mathcal{U}_{C_1}$ *be a closed subset of*

$$\mathcal{U}_{C_4}:=\left\{\mathbf{u}\in[H^2(\Gamma_{\mathrm{in}})]^d \;:\; \|\mathbf{u}\|_2\le C_4\right\} \tag{2.2}$$

for some $C_4>0$ *small enough such that* (1.4) *is satisfied, and furthermore that the viscosity is large enough to satisfy* (1.5)*. Then the problem* (CU) *admits at least one optimal solution.*

Proof. Since Γ_{in} is a bounded domain, the embedding $H^2(\Gamma_{\mathrm{in}})\hookrightarrow H^1(\Gamma_{\mathrm{in}})$ is compact by Rellich's theorem and $\mathcal{U}_{\mathrm{in}}$ is compact in $[H^1(\Gamma_{\mathrm{in}})]^d$. According to Lemma 1.1, the solution map $\mathbf{u}_{\mathrm{in}}\mapsto\mathbf{v}(\mathbf{u}_{\mathrm{in}})$ is continuous in the H^1-topology under our assumptions. Thus the image of $\mathcal{U}_{C_4}$ given by the Navier-Stokes resolvant operator (1.2) is a compact set in $\mathcal{Y}$. A bounded upper semicontinuous functional attains its maximum in a compact set. □

It is clear that for coercive cost functionals satisfying (2.1) the maximizer of (CU) will be found on the boundary of the set of admissible functions $\mathcal{U}_{\mathrm{in}}$. Thus we expect to find maximizers that become increasingly singular as we increase C_4 in (2.2). In case a near-complete occlusion is not expected, the admissible set of residual flow functions can be regularized to rule out extreme singular cases. In this case we can use the knowledge about the solutions of the (CU) to design a reasonable set of admissible residual flow functions that still contain some level of uncertainty while being mathematically better behaved. We return to this consideration in the numerical examples section.

Existence of solutions for the worst-case problem (RD-OC) in the infinite-dimensional case has not been extensively studied. In a recent paper [27], the authors used the concept of weak lower semi-continuity for set-valued functions to prove existence results for optimal control problems of PDEs for functionals of the min-max type. In the case that the admissible set of residual flow profiles $\mathcal{U}_{\mathrm{in}}$ does not depend on the control variable $\mathbf{u}_{\mathrm{bc}}$, and therefore a sufficient condition for the weak lower semi-continuity of

$$\widehat{J}(\mathbf{u}_{\mathrm{bc}}):=\sup_{\mathbf{u}_{\mathrm{in}}\in\mathcal{U}_{\mathrm{in}}}\mathbf{J}(\mathbf{u}_{\mathrm{bc}},\mathbf{u}_{\mathrm{in}})$$

https://doi.org/10.1051/m2an/2012059 Published online by Cambridge University Press

is that $J(\cdot, \mathbf{u}_{\rm in})$ is weakly lower semi-continuous for all admissible $\mathbf{u}_{\rm in} \in \mathcal{U}_{\rm in}$ (Thm. 2.5 of [27]). This assumption of independence holds in our problem, due to the special formulation (1.3) of the flux constraint, which leads to

$$\mathcal{U}_{\rm bc} \subset \left\{ \mathbf{u} \in [H^{1/2}(\Gamma_{\rm bc})]^d \ : \qquad \int_{\Gamma_{\rm bc}} \mathbf{u} \cdot \mathbf{n} \, \mathrm{d}\Gamma \ \equiv \ 1 \right\}$$

$$\mathcal{U}_{\rm in} \subset \left\{ \mathbf{u} \in [H^{1/2}(\Gamma_{\rm in})]^d \cap \mathcal{U}_{C_4} \ : \ 0 \ \leq \ \int_{\Gamma_{\rm in}} \mathbf{u} \cdot \mathbf{n} \, \mathrm{d}\Gamma \ \leq \ Q_{\rm tot} \right\}$$

In this way the flow split is completely controlled by the unknown residual flow $\mathbf{u}_{\rm in}$.

2.2. Some remarks on the solution of min-max-type problems

Several approaches can be used for the solution of standard optimal control problems such as (DD-OC) and (CU). Standard techniques are based on iterative optimization schemes based on the gradient of the cost functional, such as the steepest descent method (in this case, at each iteration, the control variable is updated in order to step along the opposite direction of the gradient of the cost functional). This entails the repeated solution, until convergence of the procedure, of the *Euler–Lagrange system* of PDEs obtained by deriving the first order necessary optimality conditions. To derive this system, we can exploit the Lagrangian functional approach [22]: by formally differentiating the Lagrangian and looking for its stationary points, we obtain the simultaneous set of state equations, adjoint state equations, and the equation expressing the optimality condition. In contrast, the min-max problem (RD-OC) is much harder. Already in the linear finite-dimensional case (where min-max problems are a special case of the so-called *bilevel programming* problem [13, 59]) it is known that the feasible set is in general nonconvex and solutions can fail to exist. The straightforward trick of treating the min-max problem as an optimization problem with a semismooth cost function, i.e.

$$\min_{\mathbf{u}_{\rm bc} \in \mathcal{U}_{\rm bc}} \ \Psi(\mathbf{u}_{\rm bc}),$$

where

$$\Psi(\mathbf{u}_{\rm bc}) := \max_{\mathbf{u}_{\rm in} \in \mathcal{U}_{\rm in}} J(\mathbf{v}) \quad \text{s.t. } \mathcal{A}(\mathbf{v}, p, \boldsymbol{\eta}; \mathbf{z}, q, \boldsymbol{\lambda}; \mathbf{u}_{\rm bc}, \mathbf{u}_{\rm in}) = 0, \quad \forall\, (\mathbf{z}, q, \lambda) \in \mathcal{Y} \times \mathcal{Q} \times \mathcal{G}, \tag{2.3}$$

runs into the possibility that $\Psi(\mathbf{u}_{\rm bc}) = +\infty$ if the inner problem is infeasible. In the case that the inner problem is convex and admits a unique solution for every $\mathbf{u}_{\rm bc} \in \mathcal{U}_{\rm bc}$, one can attempt to replace the solution of the inner optimization problem with its necessary and sufficient KKT conditions

$$\frac{\partial \mathcal{L}}{\partial \mathbf{z}}(\mathbf{v}, p, \boldsymbol{\eta}; \mathbf{z}, q, \boldsymbol{\lambda}; \mathbf{u}_{\rm bc}, \mathbf{u}_{\rm in}) = 0, \quad \frac{\partial \mathcal{L}}{\partial \mathbf{v}}(\mathbf{v}, p, \boldsymbol{\eta}; \mathbf{z}, q, \boldsymbol{\lambda}; \mathbf{u}_{\rm bc}, \mathbf{u}_{\rm in}) = 0, \quad \frac{\partial \mathcal{L}}{\partial \mathbf{u}_{\rm in}}(\mathbf{v}, p, \boldsymbol{\eta}; \mathbf{z}, q, \boldsymbol{\lambda}; \mathbf{u}_{\rm bc}, \mathbf{u}_{\rm in}) = 0 \tag{2.4}$$

expressed using the Lagrangian for the inner problem

$$\mathcal{L}(\mathbf{v}, p, \boldsymbol{\eta}; \mathbf{z}, q, \boldsymbol{\lambda}; \mathbf{u}_{\rm bc}, \mathbf{u}_{\rm in}) := -J(\mathbf{v}) - \mathcal{A}(\mathbf{v}, p, \boldsymbol{\eta}; \mathbf{z}, q, \boldsymbol{\lambda}; \mathbf{u}_{\rm bc}, \mathbf{u}_{\rm in}).$$

Then one ends up with an optimal control problem in the form

$$\min_{\mathbf{u}_{\rm bc} \in \mathcal{U}_{\rm bc}} J(\mathbf{v}) \quad \text{s.t.} \quad \begin{cases} \dfrac{\partial \mathcal{L}}{\partial \mathbf{z}}(\mathbf{v}, p, \boldsymbol{\eta}; \mathbf{z}, q, \boldsymbol{\lambda}; \mathbf{u}_{\rm bc}, \mathbf{u}_{\rm in}) = 0 \\ \dfrac{\partial \mathcal{L}}{\partial \mathbf{v}}(\mathbf{v}, p, \boldsymbol{\eta}; \mathbf{z}, q, \boldsymbol{\lambda}; \mathbf{u}_{\rm bc}, \mathbf{u}_{\rm in}) = 0 \\ \dfrac{\partial \mathcal{L}}{\partial \mathbf{u}_{\rm in}}(\mathbf{v}, p, \boldsymbol{\eta}; \mathbf{z}, q, \boldsymbol{\lambda}; \mathbf{u}_{\rm bc}, \mathbf{u}_{\rm in}) = 0 \end{cases},$$

where the adjoint state equations and the optimality conditions of the inner problem enter as additional constraints of the outer problem. This then necessitates at each optimization iteration the solution of the KKT

https://doi.org/10.1051/m2an/2012059 Published online by Cambridge University Press

conditions present in the constraints, either using a one-shot method for the coupled state-adjoint-optimality system, or some type of iterative solution algorithm.

In our boundary control formulation the inner problem is not convex, but nevertheless Theorem 2.2 guarantees the solvability of the inner problem (2.3). In the numerical examples of the boundary control formulation, we focus mainly on the optimization of the anastomosis angle, *i.e.* $\mathbf{u}_{\mathrm{bc}} = \mathbf{u}_{\mathrm{bc}}(\theta)$, where $\theta_{\min} \leq \theta \leq \theta_{\max}$ is the anastomosis angle. Provided that the functional $\Psi(\theta) = \Psi(\mathbf{u}_{\mathrm{bc}}(\theta))$ defined according to (2.3) is unimodal w.r.t the anastomosis angle θ, we can apply the golden section method [8] for derivative-free optimization of the outer problem. Each evaluation of $\Psi(\theta)$ then requires the solution of the inner problem, which we perform by a black-box implementation (Matlab's `fmincon`) of affine-scaling interior-point Newton methods [11] for nonlinear programming with box constraints.

3. A robust shape optimization formulation for bypass design

An alternative approach for the optimal design of bypass grafts relies on the solution of a shape optimization (SO) problem, for which the control variable is the shape of the domain Ω itself. This entails the minimization of a cost functional by finding the optimal shape of the domain where the PDE is defined. In general, this problem features more difficulties than OC problems, such as shape deformation, shape derivatives and the evaluation of shape-dependent quantities; a crucial aspect is the geometrical treatment of the shapes during the optimization process too.

In an abstract setting, our problem can be formulated as the following *deterministic design (SO)* problem:

$$\min_{\Omega\in\mathcal{O}_{\mathrm{ad}}} J(\mathbf{v};\Omega,\mathbf{u}_{\mathrm{in}}) \quad \text{s.t.} \quad \mathcal{A}(\mathbf{v},p,\boldsymbol{\eta};\mathbf{z},q,\boldsymbol{\lambda};\Omega,\mathbf{u}_{\mathrm{in}})=0, \quad \forall\,(\mathbf{z},q,\boldsymbol{\lambda})\in\mathcal{Y}(\Omega)\times\mathcal{Q}(\Omega)\times\mathcal{G}(\Omega), \tag{DD-SO}$$

where $\mathbf{u}_{\mathrm{in}}$ is a given residual flow function, $\mathcal{O}_{\mathrm{ad}} \subseteq \mathcal{O}$ denotes a set of admissible shapes among family of all possible shapes $\mathcal{O}$ (to be specified next). The dependence of the state equation and the cost functional on the domain Ω has now been made explicit. As in the optimal control case, a second interesting shape optimization problem is that of a bypass graft design which is *robust* with respect to the residual flow $\mathbf{u}_{\mathrm{in}}$ across the occluded branch. In this case, finding the optimal shape of the graft in presence of the worst case scenario in terms of residual flow consists in solving the following *robust design (SO)* problem:

$$\min_{\Omega\in\mathcal{O}_{\mathrm{ad}}} \max_{\mathbf{u}_{\mathrm{in}}\in\mathcal{U}_{\mathrm{in}}} J(\mathbf{v};\Omega,\mathbf{u}_{\mathrm{in}}) \quad \text{s.t.} \quad \mathcal{A}(\mathbf{v},p,\boldsymbol{\eta};\mathbf{z},q,\boldsymbol{\lambda};\Omega,\mathbf{u}_{\mathrm{in}})=0, \quad \forall\,(\mathbf{z},q,\lambda)\in\mathcal{Y}(\Omega)\times\mathcal{Q}(\Omega)\times\mathcal{G}(\Omega), \tag{RD-SO}$$

Verifying the well-posedness of shape optimization problems involves additional assumptions of regularity on admissible shapes and continuity of the state solution with respect to shape deformations. Provided that in any domain $\Omega \in \mathcal{O}$ we can solve the state problem uniquely, we can introduce a mapping U that with any $\Omega \in \mathcal{O}$ associates the state solution $U(\Omega) = (\mathbf{v},p)(\Omega)$, *i.e.* $U : \Omega \mapsto U(\Omega) \in \mathcal{V}(\Omega)$. Moreover, let $\{\Omega_n\}_{n=1}^{\infty} \subset \mathcal{O}$ be a sequence converging to $\Omega^* \in \mathcal{O}$, $U_n \equiv U(\Omega_n) \in \mathcal{V}(\Omega_n)$; denote as well $\Omega_n \xrightarrow{\tau} \Omega^*$ and $U_n \rightsquigarrow U$ two suitable notions of convergence. (in the latter case convergence involves different functional spaces, defined on the sequence $\{\Omega_n\}_{n=1}^{\infty}$). Focusing for the sake of simplicity on the shape optimization problem (DD-SO), for a given residual flow $\mathbf{u}_{\mathrm{in}}$, the following existence result holds (see for example [26], Thm. 2.10):

Theorem 3.1. *Let $\mathcal{G} = \{(\Omega, U(\Omega)), \forall\,\Omega \in \mathcal{O}_{\mathrm{ad}}\}$ be the graph of the mapping $U(\cdot)$ restricted to $\mathcal{O}_{\mathrm{ad}}$. Assume that:*

(*i*) *$\mathcal{G}$ is compact,* i.e. *for any sequence $\{(\Omega_n, U(\Omega_n)) \in \mathcal{G}\}_{n=1}^{\infty}$, there exists a subsequence, denoted with $\{(\Omega_{n_k}, U(\Omega_{n_k})) \in \mathcal{G}\}_{k=1}^{\infty}$, and an element $(\Omega^*, U(\Omega^*)) \in \mathcal{G}$, such that $\Omega_{n_k} \xrightarrow{\tau} \Omega^*$, $U(\Omega_{n_k}) \rightsquigarrow U(\Omega^*)$ for $k \to \infty$;*

(*ii*) *the cost functional $J(U;\Omega)$ is lower semicontinuous,* i.e. *if $\Omega_n \xrightarrow{\tau} \Omega^*$ and $U_n \rightsquigarrow U^*$, then $\liminf_{n\to\infty} J(U_n;\Omega_n) \geq J(U^*;\Omega^*)$.*

Then problem (DD-SO) has at least one solution.

https://doi.org/10.1051/m2an/2012059 Published online by Cambridge University Press

We point out that the first assumption of the theorem is usually shown by proving (*i*.a) the compactness of $\mathcal{O}_{\rm ad}$ in the topology τ and (*i*.b) the continuity of the state solution $U(\Omega)$ with respect to shape variation, *i.e.* if $\Omega_n \xrightarrow{\tau} \Omega^*$ then $U(\Omega_n) \rightsquigarrow U(\Omega^*)$. Not only, in order to show the continuity of the state solution w.r.t. shape, additional regularity properties have to be introduced on the set of admissible shapes; with this respect, a common assumption is to consider the family $\mathcal{O} \equiv \mathcal{O}_\varepsilon$ of domains with a uniformly Lipschitz boundary (or that equivalently satisfy the so-called uniform ε-cone condition [26]). Additional constraints (*e.g.* on the volume of the admissible domains) might also be imposed. See *e.g.* [24] for more details in the Navier-Stokes case.

Compactness of the set $\mathcal{O}_{\rm ad}$ can be obtained straightforward if the admissible shapes are obtained from a reference domain through deformations described by perturbations of the identity, *i.e.* if $\mathcal{O}_{\boldsymbol{\theta}} = \{\Omega = T(\tilde{\Omega}) = (I + \boldsymbol{\theta})(\tilde{\Omega})\}$ being $\boldsymbol{\theta}$ a regular vectorial field whose norm $\|\boldsymbol{\theta}\|_{W^{1,\infty}} < 1$ (see *e.g.* [3], Lem. 6.13); this will be the case of the Free-Form Deformation (FFD) technique, exploited in the numerical tests presented in Section 6.

The numerical solution of a shape optimization problem can be obtained by the same approach used for optimal control problems. Additional difficulties arise from shape-dependent quantities: for example, the shape derivative of the cost functional, which provides the optimality condition and depends *a priori* on the shape derivatives of state variables, can be written in a simpler way by exploiting the adjoint problem. The shape deformation stage during optimization requires special care, several techniques may be used in this respect.

4. Computational and geometrical reduction strategies

In practice, for both optimal control and shape optimization problems the standard adjoint-based approach will be too computationally expensive. Substantial computational saving becomes possible thanks to a *reduced order model* (ROM) which relies on two reduction steps: (i) parametrization of the control variables and (ii) substitution of the full-order finite element (FE) solution of (1.2) with a reduced solution obtained by the reduced basis (RB) method [57]. The approximation of viscous steady nonlinear flows through RB methods was first pioneered in [48] and has been analyzed in [14,15,52,61]; more recent applications can be found *e.g.* in [44] or in [35], where this approach was applied to a problem of femoral bypass graft shape optimization.

First of all we express the *control* functions (either boundary data $\mathbf{u}_{\rm bc} = \mathbf{u}_{\rm bc}(\boldsymbol{\pi})$ or admissible shapes $\Omega = \Omega(\boldsymbol{\pi})$) as a set of *parametric inputs*, depending on p *control parameters* $\boldsymbol{\pi} \in \mathcal{P} \subset \mathbb{R}^p$. This stage is straightforward in the former case, while in the latter a suitable parametrization of the geometry (as well as a change of variable) is required. Besides, uncertainty elements are treated as parametrized quantities too, depending on q additional parameters $\boldsymbol{\omega} \in \mathcal{Q} \subset \mathbb{R}^q$. In this way, an equivalent parametrized formulation of the deterministic design problems (DD-OC) or (DD-SO) can be derived as follows:

$$\min_{\boldsymbol{\pi}\in\mathcal{P}} J(V(\boldsymbol{\mu});\boldsymbol{\mu}) \quad \text{s.t.} \quad \mathcal{A}(V(\boldsymbol{\mu}), W; \boldsymbol{\mu}) = 0, \quad \forall W \in \mathcal{V}(\tilde{\Omega}), \tag{4.1}$$

where $\boldsymbol{\mu} = (\boldsymbol{\pi}, \boldsymbol{\omega}) \in \mathcal{P} \times \mathcal{Q}$, $V(\boldsymbol{\mu}) = (\mathbf{v}, p, \boldsymbol{\eta})(\boldsymbol{\mu})$, $\mathcal{V}(\tilde{\Omega})$ is a functional space defined on a reference, parameter independent domain $\tilde{\Omega}$ as $\mathcal{V}(\tilde{\Omega}) = \mathcal{Y}(\tilde{\Omega}) \times \mathcal{Q}(\tilde{\Omega}) \times \mathcal{G}(\tilde{\Omega})$. In an optimal control context, $\Omega \equiv \tilde{\Omega}$, while for a shape optimization problem the parametrized domain $\Omega = \Omega(\boldsymbol{\pi})$ is obtained by applying a parametric mapping $T(\cdot;\boldsymbol{\pi})$ to the reference domain. In our case, this map will be built by exploiting the *free-form deformation* (FFD) technique, in which the deformations of an initial design, rather than the geometry itself, are parametrized [36,43]. In the same way, the robust design problems (RD-OC) or (RD-SO) can be written as follows:

$$\min_{\boldsymbol{\pi}\in\mathcal{P}} \max_{\boldsymbol{\omega}\in\mathcal{Q}} J(V(\boldsymbol{\mu});\boldsymbol{\mu}) \quad \text{s.t.} \quad \mathcal{A}(V(\boldsymbol{\mu}), W; \boldsymbol{\mu}) = 0, \quad \forall W \in \mathcal{V}(\tilde{\Omega}). \tag{4.2}$$

Then, we replace the expensive, full-order FE solution $V_h(\boldsymbol{\mu})$ of (1.2) with the inexpensive RB solution; in the case of deterministic OC/SO problems, following the *discretize-then-optimize* approach, the standard Galerkin FE approximation of (4.1) is as follows:

$$\min_{\boldsymbol{\pi}\in\mathcal{P}} J_h(V_h(\boldsymbol{\mu});\boldsymbol{\mu}) \quad \text{s.t.} \quad \mathcal{A}(V_h(\boldsymbol{\mu}), W_h; \boldsymbol{\mu}) = 0, \quad \forall W_h \in \mathcal{V}_h(\tilde{\Omega}), \tag{4.3}$$

https://doi.org/10.1051/m2an/2012059 Published online by Cambridge University Press

where $\mathcal{N} = \mathcal{N}(h)$ is the dimension of the FE space, depending on the mesh size h. The reduced basis method (see [53,57] for reviews of the method) provides an efficient way to compute an approximation $V_N(\boldsymbol{\mu})$ of $V_h(\boldsymbol{\mu})$ (and related output) by using a Galerkin projection on a reduced subspace made up of well-chosen FE solutions, corresponding to a specific choice $S_N = \{\boldsymbol{\mu}^1, \ldots, \boldsymbol{\mu}^N\}$ of parameter values. Indicating by $\mathcal{V}_N = \text{span}\{V_h(\boldsymbol{\mu}^n), n = 1, \ldots, N\}$ the RB space, the RB formulation of (4.3) is as follows:

$$\min_{\boldsymbol{\pi} \in \mathcal{P}} J_N(V_N(\boldsymbol{\mu}); \boldsymbol{\mu}) \quad \text{s.t.} \quad \mathcal{A}(V_N(\boldsymbol{\mu}), W_N; \boldsymbol{\mu}) = 0, \quad \forall\, W_N \in \mathcal{V}_N. \tag{4.4}$$

Thanks to the (considerably) reduced dimension $N \ll \mathcal{N}$ of the space obtained from RB approximation – in our cases, $N \approx 10$, whereas $\mathcal{N} > 10^4$ – we can provide *rapid responses* in terms of input/output evaluations. This is ensured by an Offline-Online computational strategy and a rapidly convergent RB space assembling, based on a *greedy algorithm* [57]. More precisely, in an expensive Offline stage we prepare a very small RB "database", while in the Online stage, for each new $\boldsymbol{\mu} \in \mathcal{D}$, we rapidly evaluate both the solution and the output. At the outer level, a suitable iterative optimization procedure is performed, now involving a very reduced version of the original problem. On the other hand, the *reliability* of the RB method is ensured by rigorous a posteriori estimations for the error in the RB approximation w.r.t. truth FE discretization [57]. See *e.g.* [14,15,42,61] for the derivation of a posteriori error bounds in the case of Navier-Stokes equations, based on the Brezzi−Rappaz−Raviart theory.

5. Numerical results: boundary optimal control

In this section we present some numerical results about the optimal design of aorto-coronary bypass grafts based on the solution of the optimal control problems analyzed in Section 2.

5.1. Two-dimensional boundary control problems

We consider throughout this section a simplified 2D bypass configuration $\Omega = (0,5) \times (0,1)$, where $\Gamma_{\text{in}} = \{(x,y) : x = 0,\ y \in (0,1)\}$ and $\Gamma_{\text{bc}} = \{(x,y) : x \in (1,3/2),\ y = 1\}$, respectively, thus considering the graft-to-host diameter ratio to be fixed at its (near-)optimal value 1.5 as discussed in [32].

In order to exploit the reduced framework discussed in the previous section, we make the simplifying assumption that the control functions are parametrized with respect to the anastomosis angle θ and are given by the following parabolic Poiseuille profiles for simplicity[10]:

$$\mathbf{u}_{\text{bc}}(x; \theta, \omega) := \frac{16}{9}\left(\frac{7}{6} - \frac{\omega}{6}\right)\left(x - 1\right)\left(\frac{3}{2} - x\right)\begin{bmatrix}(\tan\theta)^{-1}\\ -1\end{bmatrix}, \tag{5.1}$$

where $\theta \in (\theta_{\min}, \theta_{\max})$ and $0 < \theta_{\min} < \theta_{\max} \leq \pi/2$. In this way, the set of admissible[11] boundary controls is defined by $\mathcal{U}_{\text{bc}} := \{\mathbf{u}_{\text{bc}}(x; \theta, \omega) :\ \theta \in [\theta_{\min}, \theta_{\max}]\}$, being in our case $\theta_{\min} = 15°$ and $\theta_{\max} = 85°$. On the other hand, $\omega \in (0,4)$ is the variable controlling the flux split between the graft and the host vessels: if $\omega = 0$ we have a completely occlusion, while for $\omega = 4$ we have a 50/50 split of total flux between the graft and the host. The control function $\mathbf{u}_{\text{bc}}$ is properly rescaled to satisfy (1.3).

Thus the control variable in the simplified deterministic design problem is reduced to the angle θ of the bypass graft. Also the radius of the bypass could be taken as an optimization variable, in the case that this is under control of the surgeon performing the operation, but in general more complex geometrical properties such as cuff shapes cannot be incorporated into our model problem. Clearly, we are interested in the minimization of the cost functionals J_1 – J_4 in the downfield subregion Ω_{obs} where a vortex may occur, leading to possible occlusions after grafting and plaque formation; here $\Omega_{\text{obs}} = \{(x,y) \in \Omega\ :\ (x,y) \in (1,4) \times (0,1)\}$ (see Figs. 1, 2). The

[10] For small angles θ our choice results in unrealistic inflow profiles with small graft diameter, and should only be used for angles above, say, $\theta_{\min} \geq 20°$. In practice the optimal angles found were outside this critical range of small angles.

[11] Concerning the existence results provided in Section 2, it is clear that the admissible set $\mathcal{U}_{\text{bc}}$ given by the control functions (5.1) is closed in $H^{1/2}(\partial\Omega)$. To see that it is also convex, note that $\varphi(\theta) = 1/\tan\theta$ is a continuous function in $\theta \in [\theta_{\min}, \theta_{\max}]$ and its image is a closed interval, therefore convex.

https://doi.org/10.1051/m2an/2012059 Published online by Cambridge University Press

resulting problem is discretized with 14 260 and 1827 dofs for velocity and pressure, respectively, using $\mathbb{P}_2/\mathbb{P}_1$ finite elements; the dimension of the computed reduced basis space is $N = 54$, thus yielding the possibility to solve a Navier-Stokes problem in a *real time* way (averaged time over 1,000 evaluations is 0.19 seconds). Parametric optimization was performed by derivative-free golden section method for the outer problem and by a black-box implementation (Matlab's `fmincon`) of affine-scaling interior-point Newton methods [11] for nonlinear programming with box constraints for the inner problem.

5.1.1. Deterministic design optimal control problem

As a first approximation we assume that the residual flow profile is parabolic, in particular it is defined as $\mathbf{u}_{\text{in}}(\mathbf{y};\omega) := \omega\mathbf{y}(\mathbf{1}-\mathbf{y})\mathbf{e_1}$. This is a typical choice in numerical simulations of arteries yet its justification or effect on the outcomes seems to be rarely considered. We have solved the (DD-OC) problem for 7 different values of $\omega \in [0,3]$ and for 6 different values of the Reynolds number $Re \in (15,90)$ considered as a further input parameter in the formulation (1.1); nevertheless, for the sake of simplicity we report here the results for the maximum value experimented, Re = 90. Within the reduced framework illustrated, the solution of 42 optimal control problems takes about 3 hours of CPU time[12], each of them implying about $10 \div 15$ iterations of the optimization procedure.

The optimal angle θ^* obtained by solving the problem (DD-OC) decreases as the magnitude of the residual flow increases. The specific behavior and values of the four cost functionals varies, however, leading to different ranges for $\theta^* = \theta^*(\omega)$. In particular, the vorticity functional J_3 and the Stokes tracking functional J_2 (see Fig. 3) exhibit a stronger convexity and lead to smaller values of the optimal angles: $\theta^* \in (29°, 43°)$ for J_3 and $\theta^* \in (27°, 30°)$ for J_2, respectively, which are very close to values usually treated as optimal for a graft anastomosis [39,58]. On the other hand, minimization of functionals J_1 and J_4 yields larger values of the optimal angles, perhaps due to their weaker convexity. In Figure 4 the flows corresponding to the optimal angles for the functional J_3 and $\omega = 0$, $\omega = 1$ are represented. We point out that in the case of total occlusion the main vortex core in the heel region can never be totally eliminated.

5.1.2. Complementary uncertainty optimal control problem

Since the residual flow profile in the (partially) occluded artery might play an important role in the fluid dynamics of a bypass model, instead of using the parabolic profile $\mathbf{u}_{\text{in}}$ we are interested in finding the profile of the worst residual flow so that the optimized graft is *robust* not just to the magnitude of this flow, but also to its profile. To this aim, we solve a relaxed version of the (CU) problem[13], by considering parametrized control functions $\mathbf{u}_{\text{in}}$ under the form

$$\mathbf{u}_{\text{in}}(y;\boldsymbol{\pi}) = \sum_{i=1}^{6} \pi_i \boldsymbol{\phi}_i(y)\mathbf{e}_1$$

being $\boldsymbol{\phi}_1$ the parabolic profile already introduced, $\boldsymbol{\phi}_2 = \exp(-100(y-0.5)^2)$, $\boldsymbol{\phi}_3 = \exp(-100(y-0.25)^2)$, $\boldsymbol{\phi}_4 = \exp(-100(y-0.75)^2)$ three gaussian profiles centered at the points 0.25, 0.5 and 0.75, and $\boldsymbol{\phi}_5 = y(1-y)(y-0.25)$, $\boldsymbol{\phi}_6 = y(1-y)(y-0.75)$ two cubic profiles, where the control parameters $\{\boldsymbol{\pi}_i\}_{i=1}^6$ are such that the flux of $\mathbf{u}_{\text{in}}$ is constant. By solving the relaxed (CU) problem, we find that the worst case corresponds to the gaussian profile centered at the midpoint of the occluded section $y = 0.5$, thus corresponding to a severe occlusion in the host artery. The function $\mathbf{u}_{\text{in}} = \omega \exp(-100y^2)\mathbf{e}_1$ will be the boundary condition on Γ_{in} from now on.

5.1.3. Robust design optimal control problem

We can now solve the robust design (RD-OC) problem by considering the same setting as in the (DD-OC) case and the residual flow $\mathbf{u}_{\text{in}}$ given by the gaussian profile obtained by solving the complementary uncertainty (CU) problem. First of all, we consider the deterministic design (DD-OC) problem with a gaussian residual flow: the results, concerning the behavior of the vorticity functional J_3 w.r.t. θ and ω, as well as the optimal angles

[12] Computations involving RB approximations have been executed on a personal computer with 2 × 2GHz Dual Core AMD Opteron (tm) processors 2214 HE and 16 GB of RAM.

[13] The full RB adjoint-based method for the solution of (CU) is unavailable at this time.

https://doi.org/10.1051/m2an/2012059 Published online by Cambridge University Press

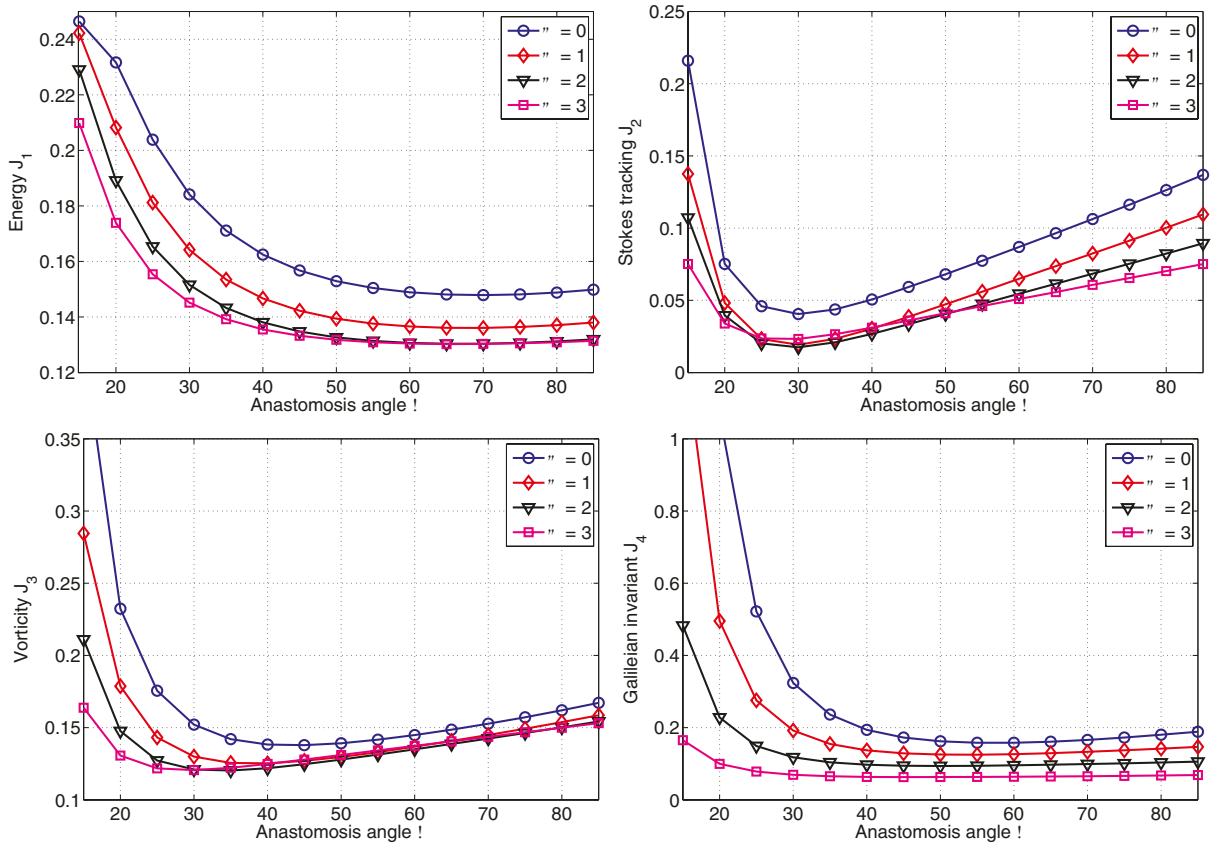


FIGURE 3. Functionals J_1, J_2, J_3, and J_4 in the subdomain as a function of the anastomosis angle θ for different values of the residual parameter ω with parabolic residual flow.

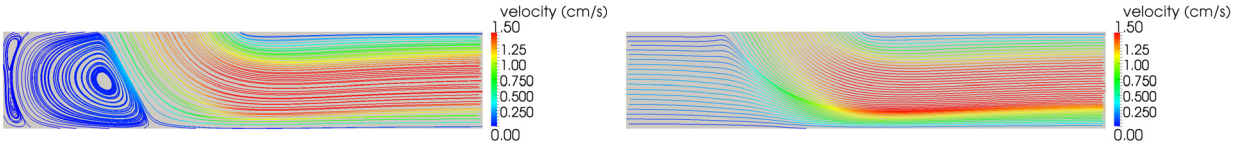


FIGURE 4. Flow in the optimal configuration for the cost functional J_3, $\omega = 0$ (left) and $\omega = 1$ (right), with parabolic residual flow.

obtained with the four functionals $J_1 - J_4$, are reported in Figure 5 for both the parabolic and gaussian residual inflows. The results follow the same trends in both cases, even if flow patterns are remarkably different if the residual flow profile changes. In particular, the gaussian profile induces two secondary vortices near the occlusion, and a more complex vorticity pattern in the anastomosis region.

Two major sources of vorticity can be observed from the streamlines. The first one is the primary vortex behind the incoming jet, which is generated by the interaction between the fast and slow flows coming into contact at the anastomosis exit. This vortex tends to disappear as we increase ω (see Figs. 4 and 6). Secondary vortices are generated by the peak residual flow on both sides of the entry from the occluded branch. However,

https://doi.org/10.1051/m2an/2012059 Published online by Cambridge University Press

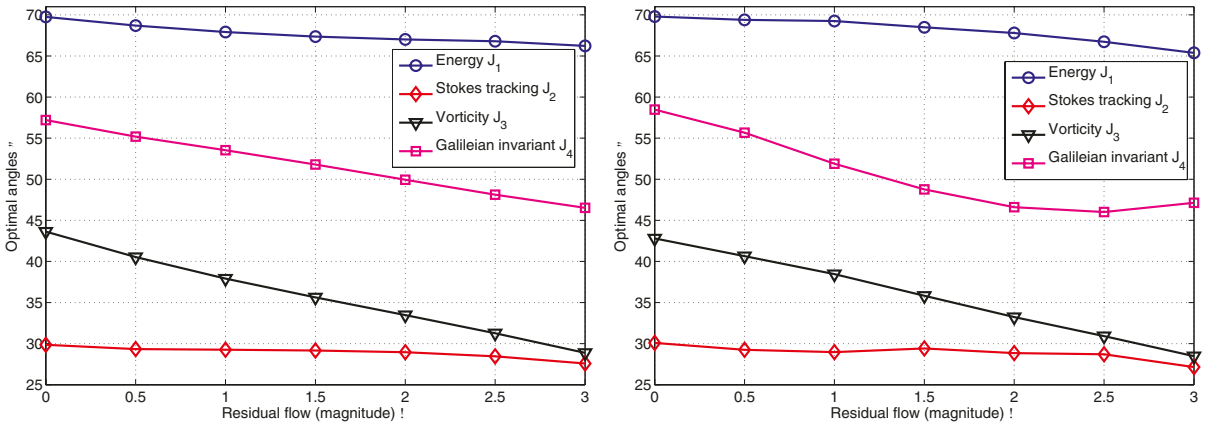


FIGURE 5. Optimal anastomosis angles as a function of the residual parameter ω for the functionals J_1 – J_4, for the parabolic residual flow (left) and the gaussian residual flow (right).

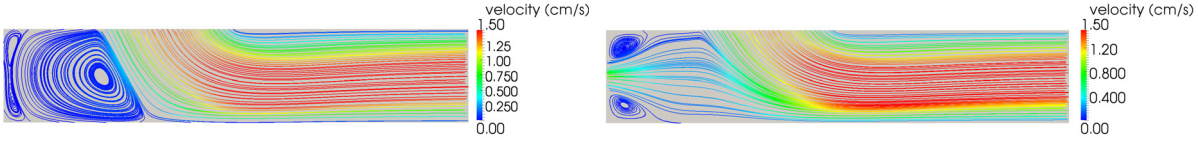


FIGURE 6. Flow in the optimal configuration for the cost functional J_3, $\omega = 0$ (left) and $\omega = 1$ (right), with gaussian residual flow.

TABLE 1. Optimal angles and robust angles θ^* obtained through the (DD-OC) and (RD-OC) problems, Stokes tracking functional J_2 and vorticity functional J_3, both in 2D and 3D.

Functional	Dimension	Profile	$\omega = 0$	$\omega = 1$	$\omega = 2$	$\omega = 3$	Robust solution
J_3	2D	$\mathbf{u}_{\text{in}}$ parabolic	43.6	37.9	33.4	28.9	–
	2D	$\mathbf{u}_{\text{in}}$ gaussian	42.8	38.5	33.2	28.5	42.6
J_2	2D	$\mathbf{u}_{\text{in}}$ parabolic	29.9	29.2	28.9	27.5	–
	2D	$\mathbf{u}_{\text{in}}$ gaussian	30.1	28.9	28.8	27.1	30.0
J_3	3D	$\mathbf{u}_{\text{in}}$ gaussian	45.8	43.8	41.4	38.0	–

due to the choice of the observation subdomain, which considers only the flow downstream from the anastomosis, their effect is removed from the vorticity measure: this explains why the results, in terms of optimal angles, are very similar.

In Figure 6 the flows corresponding to the optimal angles for the functional J_3 and $\omega = 0, 1$ are represented. Finally, the robust design problem (RD-OC) has been solved for the four cost functionals J_1 – J_4, providing the results listed in Table 1 (dealing with the most significant J_3 and J_2 cases). Each of these four problems takes approximately $500 \div 700$ seconds to be solved, requiring about $110 \div 150$ input/output evaluations, depending on each case. The robust angles are about the same as the ones obtained as solutions of the deterministic design (DD-OC) problem in the case $\omega = 0$. Hence, the most challenging situation for the minimization of vorticity appears to be the case of total or near-total occlusion of the stenosed branch.

https://doi.org/10.1051/m2an/2012059 Published online by Cambridge University Press

5.2. Comparison with three-dimensional steady flow

The three-dimensional effects in a steady flow through a bypass anastomosis were considered in [19] and found to be highly significant when it comes to the WSS distribution, especially at higher Reynolds numbers. To test the relevance of 3D effects on the optimal anastomosis angle in our simplified setup, we consider a 3D problem which is assumed plane symmetric along the centerline of the vessel – thus only the half-width of the configuration needs to be meshed. The axisymmetric setting was done in order to obtain results that are comparable with the 2D case. The length and radius of the channel and the bypass are kept the same as in the 2D case, as well as the inflow profiles, which are chosen to be radially symmetric:

$$\mathbf{u}_{\text{in}}(\mathbf{y},\mathbf{z};\omega) := \omega \exp\left[-100\left(y^2+z^2\right)\right],$$
$$\mathbf{u}_{\text{bc}}(\mathbf{x},\mathbf{z};\theta,\omega) := \left(\frac{7}{6}-\frac{\omega}{6}\right)\left[1-\frac{16}{9}\left(x-\frac{7}{4}\right)^2+4z^2\right]\begin{bmatrix}(\tan\theta)^{-1}\\ -1\end{bmatrix}.$$

We also choose the viscosity in such a way that the Reynolds number is comparable to the highest possible one used in the 2D case, *i.e.* $Re \approx 80$. This is obtained correspondingly to $\nu = 0.0125\ \text{cm}^2\,\text{s}^{-1}$. The resulting problem is discretized with 196 041 and 65 347 dofs for velocity and pressure, respectively, using $\mathbb{P}_1/\mathbb{P}_1$ finite elements with an interior penalty stabilization scheme [9]. The nonlinear problem (1.1) is solved starting from the steady Stokes solution and performing pseudo-time stepping until convergence to a steady solution has been achieved. No model reduction was applied in this case and as a result each solution took roughly 20 minutes on 24 parallel 2.66 GHz cores of an Intel Xeon Nehalem cluster.

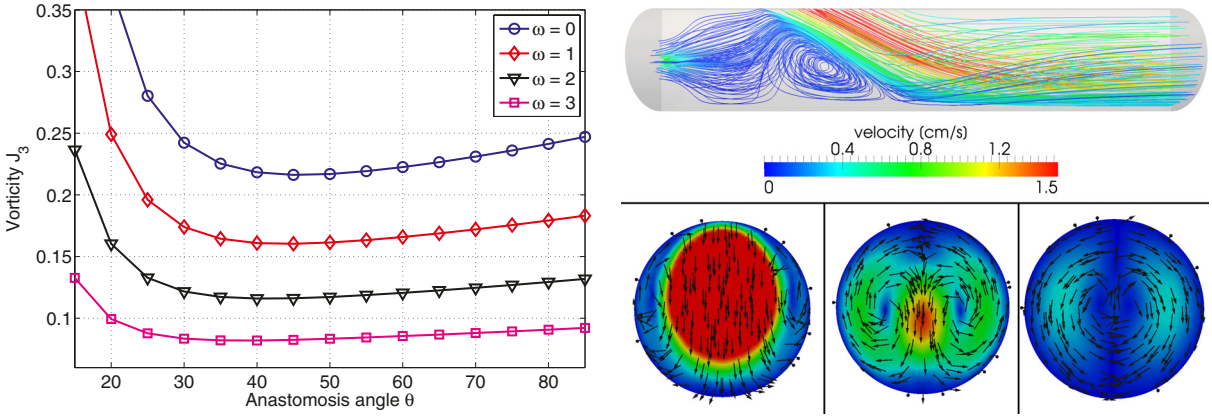
In this comparison we consider only the cost functional J_3. The energy functional J_1 is omitted, since it suggests angles that are too large to be used in practice and can cause strong localized stresses on the arterial wall due to an impinging fluid jet. The Stokes tracking functional J_2 is omitted, since nonlinear convective effects are likely to be much more significant in 3D, invalidating the comparison between Navier-Stokes and Stokes solutions. Finally, the Galileian invariant functional J_4 is only valid in 2D. In Figure 7a we display the obtained value of the vorticity functional J_3 for different values of the parameter ω. In each case the functional is convex and the optimal angle is located around 45°, but as ω increases the optimal angle θ^* decreases. The qualitative behavior of the vorticity functional J_3 resembles that of the 2D case even if the 3D flow exhibits much more complex flow phenomena, which we will attempt to explain in the following.

Visualizations of the 3D flow field are reported in Figures 7b–9. Three major sources of vortices can be observed – primary and secondary vortices already remarked for the 2D case, and a tertiary vortex structure. As before, the primary vortex tends to disappear as we increase ω (see Fig. 8); of course, in the case of total occlusion, $\omega = 0$, the primary vortex can never be totally eliminated. This fact is demonstrated in Figure 9, where we display the flow at the maximum angle $\theta = 85°$ but with two different residual flows, $\omega = 0$ (total occlusion) an $\omega = 1$ (strong occlusion). Only in the first case can the primary vortex be observed.

Secondary vortices are generated as in the 2D case by the peak residual flow on both sides of the entry from the occluded branch. Tertiary transversal vortices, the so-called Dean vortices, appear downstream of the anastomosis at moderate Reynolds numbers. While these structures appear exclusively in the 3D flow, it seems their effect on the vorticity functional is an order of magnitude less when compared to the primary vortex, and thus they do not alter the conclusions we obtained earlier based on 2D simulations. The vorticity functional J_3 therefore measures and attempts to control mainly the primary vortex.

In particular, we can remark a strong similarity on the primary and secondary vortex structures between the 2D and the 3D case, as we can remark in Figure 10, obtained for the same values of θ and ω already considered in Figure 7b–9. For $\omega \leq 1$ a very strong primary vortex is generated for small angles θ, causing a strongly convex behavior in the functional J_3 as a function of the angle, while for $\omega \geq 3$ the value of the vorticity functional becomes rather insensitive to the choice of the anastomosis angle. Thus we are able to conclude that – similarly to the 2D case – the most challenging situation for the minimization of vorticity is the case of total or near-total occlusion of the stenosed branch. We did not test the effect of the residual flow profile uncertainty on the 3D

https://doi.org/10.1051/m2an/2012059 Published online by Cambridge University Press



(a) (b)

FIGURE 7. (a) Vorticity J_3 in the subdomain Ω_{obs} as a function of the anastomosis angle θ for different values of the residual parameter ω in the 3D bypass case. (b) Streamlines of steady flow and transversal velocities at $x = 2.5$, $x = 3.5$, and $x = 4.5$ for the case $\theta = 25°$, $\omega = 1$.

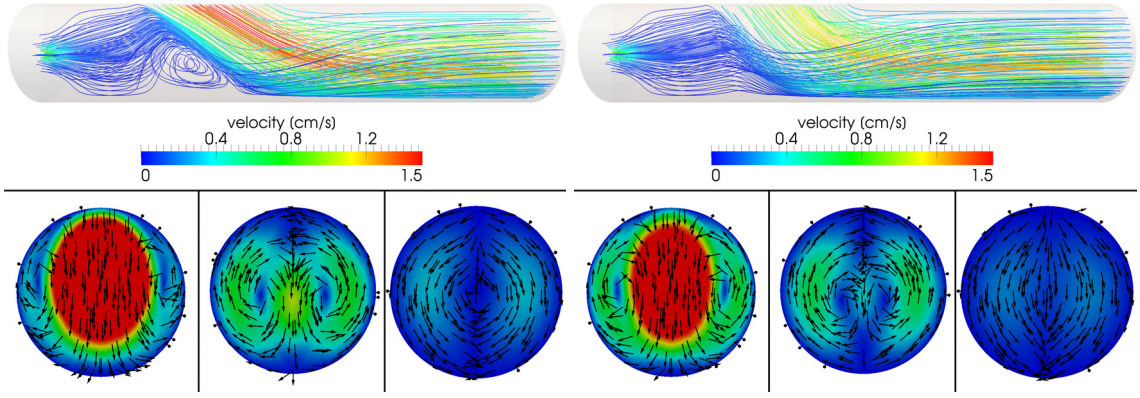


FIGURE 8. Streamlines of the steady flow and transversal velocities at $x = 2.5$, $x = 3.5$, and $x = 4.5$ for the case $\theta = 30°$ (left) and $\theta = 50°$ (right) with $\omega = 1$. For sufficiently large angles θ the primary vortex disappears, while the secondary and tertiary vortices remain.

case as the results in the 2D case already highlighted the need to consider a "worst-case" flow profile in order to obtain robust results. In Table 1 we also include the estimated optimal angles in the 3D case for reference with the 2D results presented before. These were obtained by cubic spline interpolation of the curves in Figure 7a. For $\omega = 0$ the optimal angle is very close to the one obtained for the 2D problem, while a divergence of results occurs as ω is increased; the optimal angles in the 3D case tend to be somewhat larger.

However, if the robust angle is assumed to correspond in both cases to the optimal angle for $\omega = 0$, we can state that the solution of the robust design problem in 2D gives a good indication to the choice of a robust angle in the more realistic 3D problem.

5.3. Comparison with results using wall-shear stress functionals

The remaining question to be answered is, whether the similarity of the 2D and 3D problems in the context of vorticity minimization extends also to the more difficult case of WSS-related functionals, such as J_5 given

https://doi.org/10.1051/m2an/2012059 Published online by Cambridge University Press

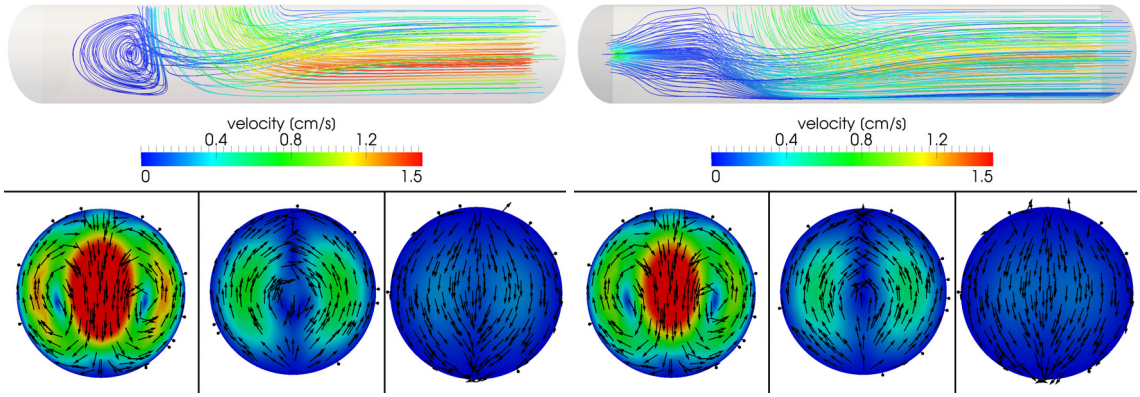


FIGURE 9. Streamlines of the steady flow and transversal velocities at $x = 2.5$, $x = 3.5$, and $x = 4.5$ for the case $\theta = 85°$ with $\omega = 0$ (left) and $\omega = 1$ (right). In the case of total occlusion, the primary vortex is present even with very large angles.

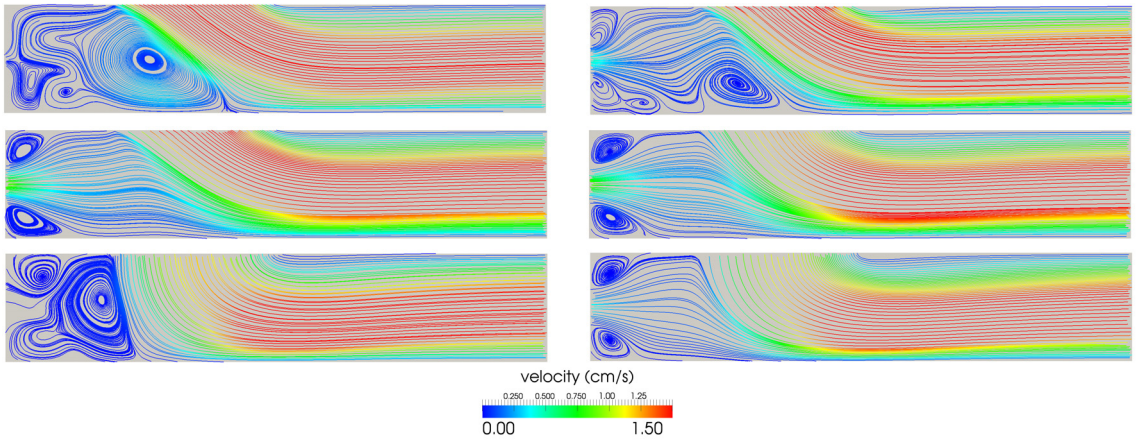


FIGURE 10. Streamlines of the 2D steady flow for the cases (from top to bottom, from left to right): $\theta = 25°$ with $\omega = 0$, $\omega = 1$; $\theta = 30°$, $\theta = 50°$ with $\omega = 0$; $\theta = 85°$ with $\omega = 0$, $\omega = 1$.

by (5). It is likely that the tertiary vortices have some effect on the downstream WSS, thus potentially changing the situation between the 2D and 3D cases. While the WSSG is sometimes used by biomechanical engineers to evaluate proposed CABG designs [37, 50], its mathematical treatment raises issues of whether sufficient regularity can be attained for the existence of minimizers. In Figure 11 we visualize the post-processed WSS for one particular case computed using $\mathbb{P}_1/\mathbb{P}_1$ finite elements. For accurate WSS computation, we performed boundary refinment on the mesh along the floor of the artery, leading to 246 339 and 82 113 dofs for velocity and pressure respectively. Velocity gradients were recovered using standard gradient recovery techniques.

A mesh convergence study was performed to guarantee that the recovered WSS quantities had converged up to a reasonable tolerance (maximum relative error <7%). As the simplified model is not sufficient to predict accurately the WSS near the heel or the toe of the anastomosis, we concentrate on the WSS along the floor. The axial component of the WSS was evaluated along a line on the floor of the host artery and is shown in Figure 12. The results obtained were qualitatively similar to those reported in [40] for experimental measurements of steady flow ($Re = 208$, WSS ≈ -5–18 dyn/cm^2). A region of low WSS forms behind the incoming flow jet, coincident

https://doi.org/10.1051/m2an/2012059 Published online by Cambridge University Press

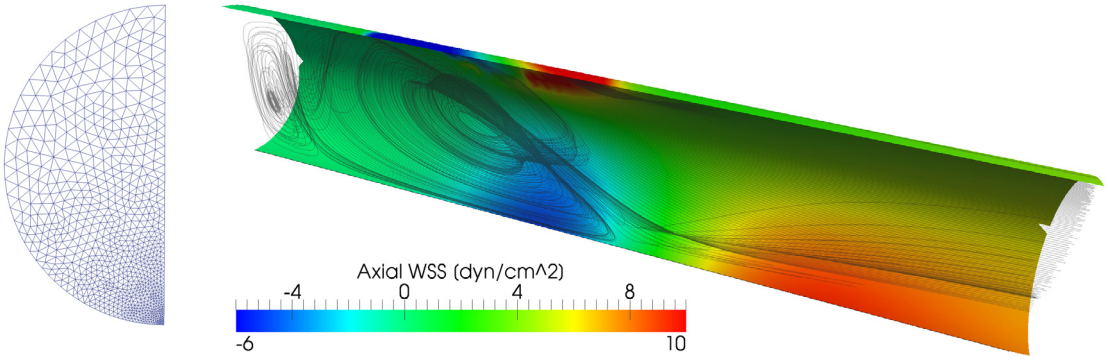


FIGURE 11. (a) Slice of the computational domain showing mesh boundary refinement along the arterial floor; (b) Visualization of the axial WSS and streamlines in the case $\omega = 0$, $\theta = 25°$.

TABLE 2. Optimal angles and robust angle θ^* obtained through the (DD-OC) and (RD-OC) problems, WSSG functional J_5, both in 2D and 3D.

Functional	Dimension	Profile	$\omega = 0$	$\omega = 1$	$\omega = 2$	$\omega = 3$	Robust solution
J_5	2D	$\mathbf{u}_{\text{in}}$ gaussian	36.5	31.2	27.7	22.6	36.4
J_5	3D	$\mathbf{u}_{\text{in}}$ gaussian	34.4	31.9	28.9	22.7	

with a strong vortex, and elevated WSS is predicted along the wall downstream from where the incoming jet impacts. We note that, due to the use of basis functions that are globally only C^0, the recovered WSS exhibits some mild numerical irregularity that might potentially hinder the evaluation of higher-order quantities such as WSSG.

A parametric study was performed to find the optimal angle in the same three cases as before. In order to compare the results with the 2D case, we only evaluated the gradient of the axial component of WSS along a line on the floor, *i.e.* the functional was reduced to

$$J_5(\mathbf{v}) \approx \int_{\Gamma_{\text{obs}}} \left| \frac{\partial(\nabla \tau_w \cdot \xi_a)}{\partial \xi_a} \right|^2 \, \mathrm{d}\Gamma,$$

which corresponds to the same one we used in the 2D case. The observation region was chosen similarly to the other functionals, *i.e.* $\Gamma_{\text{obs}} := [1, 4] \times \{-1/2\} \times \{0\}$. In Figure 13 we give the values of the J_5 functional for the four different cases: $\omega = 0, 1, 2, 3$. The optimal angles recovered are in the range 30–35° depending on the residual flow, and again the largest values of $J_5(\mathbf{v})$ were observed for the case $\omega = 0$. Moreover, the optimal angles obtained by using a 2D model are very similar to those computed by exploiting a full 3D flow simulation (see also Tab. 2). The WSSG functional was remarkably regular and convex over the parameter range despite the numerical difficulties related with reconstructing the WSSG. We finish this section by concluding that, compared to the WSSG functional, performing optimization with the vorticity functional leads to somewhat larger angles, but that both functionals can be used as indicators of low WSS regions induced by recirculation and flow stagnation.

6. NUMERICAL RESULTS: SHAPE OPTIMIZATION

Next we present results on the robust design problem using the shape optimization formulation. We consider a parametrized framework based on Free-Form Deformation (FFD), which enables the definition of a set of

https://doi.org/10.1051/m2an/2012059 Published online by Cambridge University Press

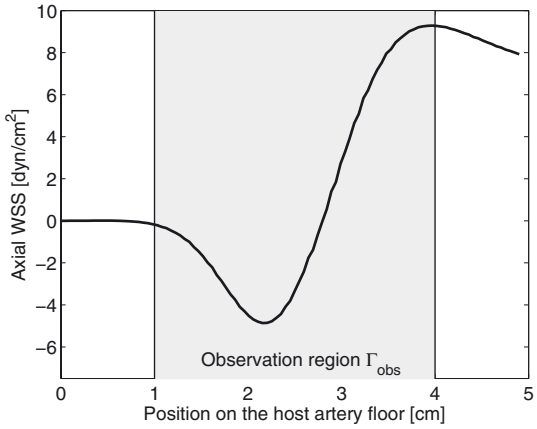
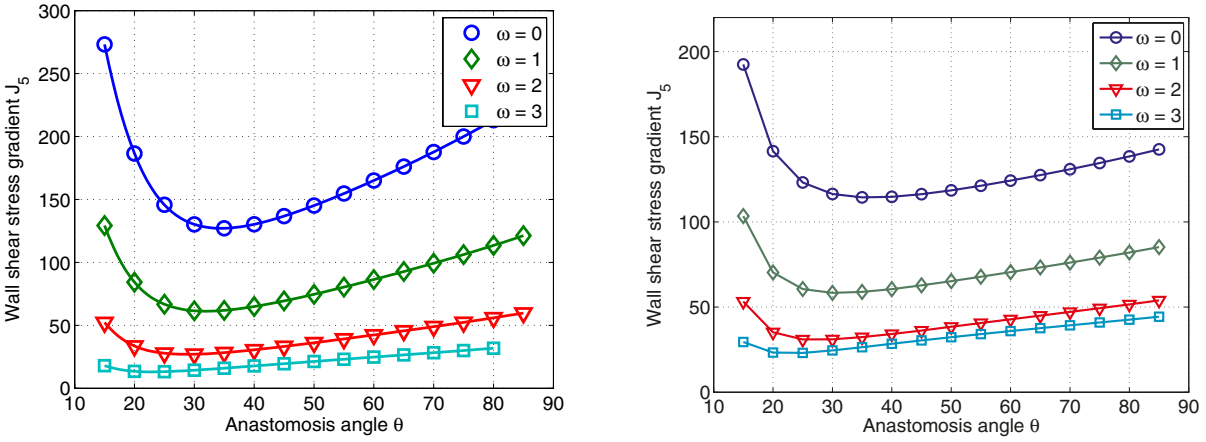


FIGURE 12. Axial component of WSS along a line on the floor of the host artery in the case $\omega = 0$, $\theta = 25°$



(a) (b)

FIGURE 13. Parametric study of the WSSG functional (5.3) for different angles (a) in the 3D case and (b) in the 2D case.

admissible shapes as diffeomorphic images of a reference graft shape $\tilde{\Omega}$ through a parametrized map $T(\cdot;\boldsymbol{\pi})$ depending on a set of control points acting as shape design parameters. The reference configuration $\tilde{\Omega}$, represented in Figure 14, has already been employed for the solution of shape optimization problems with Stokes flows in [43]. In the present case, the FFD parametrization is built on a 5×6 lattice of control points on the rectangle $D = [-1, 3] \times [-0.6, 0.4]$; active control points and their displacements are selected in order to describe a wide family of shapes in terms of the three influential geometrical features already highlighted, *i.e.* the anastomosis angle, the graft-to-host diameter ratio, and the toe shape.

In the end we use a parametrization with $p = 8$ design parameters, which represent the vertical/horizontal displacements of selected control points. These parameters vary in the range $(-\alpha, \alpha)$, $\alpha = 0.15$, for the vertical displacements and in the range $(0, \beta)$, $\beta = 0.6$, for the horizontal displacements of the control points depicted

https://doi.org/10.1051/m2an/2012059 Published online by Cambridge University Press

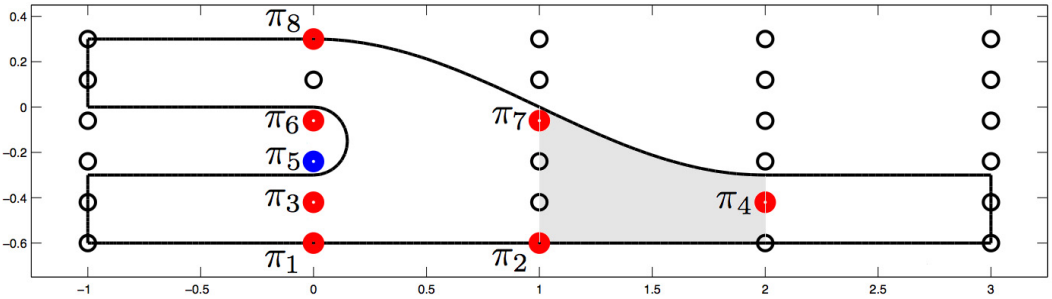


FIGURE 14. Reference domain $\tilde{\Omega}$ and FFD setting. Control points depicted in red/blue can be moved in vertical/horizontal direction.

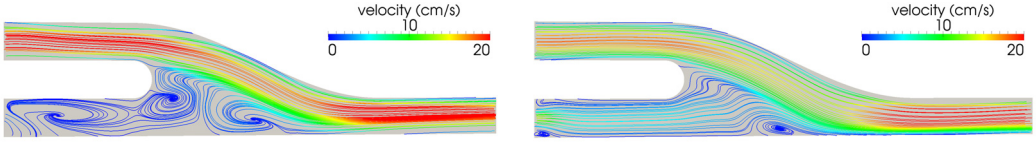


FIGURE 15. Initial shape and velocity fields in the cases $\omega = 0$ (left) and $\omega = \omega_{\max}$ (right).

in red/blue in Figure 14. As before, we consider an observation subregion close to the heel, given here by $\Omega_{\text{obs}} = \{\tilde{\mathbf{x}} = (\tilde{x}_1, \tilde{x}_2) \in \tilde{\Omega} : \tilde{x}_1 \in (1, 2)\}$ (represented in gray in Fig. 14). In this way, indicating as $\mathcal{P} = \{\boldsymbol{\pi} = (\pi_1, \ldots, \pi_8) \in \mathbb{R}^8 : \ \pi_i \in (-\alpha, \alpha) \ \ \forall\, i \neq 5, \ \pi_5 \in (0, \beta)\}$ and $V = |D|$, the set of admissible shapes is

$$\mathcal{O}_{\text{ad}} = \left\{ \Omega \subset D \subset \mathbb{R}^2 : \ \Omega = T(\tilde{\Omega}; \boldsymbol{\pi}), \quad \boldsymbol{\pi} \in \mathcal{P}, \ \Gamma_{\text{in}} \cup \Gamma_{\text{bc}} \cup \Gamma_{\text{out}} \text{ is fixed} \right\}.$$

Concerning inflow profiles, we consider a Poiseuille profile on the inflow Γ_{bc} (graft) and a parametrized gaussian profile $\mathbf{u}_{\text{in}} = \omega\phi(y)\mathbf{e}_1$ on the inflow Γ_{in} (occluded artery), being $\omega \in \mathcal{Q} = [0, \omega_{\max}]$ the uncertainty parameter tuning the degree of occlusion. In particular, the dependence of the two flows on ω is such that the downfield flowrate is constant, with a flow split ranging from 1/0 (complete occlusion of the host artery, for $\omega = 0$) to 2/1 (flowrate across the occluded artery equal to one half of the flowrate across the graft, for $\omega_{\max} = 20$). The resulting problem is discretized with 33 330 and 4269 dofs for velocity and pressure, respectively, using $\mathbb{P}_2/\mathbb{P}_1$ FE spaces; the corresponding RB approximation is defined on spaces of dimension $N = 36$, thus yielding the possibility to solve a Navier-Stokes problem in a very rapid way (1.84 s, averaged time over 1000 evaluations). Parametric optimization problems were solved through the same affine-scaling interior point Newton method exploited for the minimization problems in the OC case, using a finite difference approximation of gradients and Hessians.

In Figure 15 the velocity fields within the initial, reference shape in the cases $\omega = 0$ (complete occlusion) and $\omega = \omega_{\max}$ (maximum residual flow) are represented. In Figure 16 the velocity fields within the optimal shapes for the vorticity J_3, Stokes tracking J_2 and Galileian invariant J_4 functionals are represented, in the cases $\omega = 0$ (complete occlusion) and $\omega = \omega_{\max}$ (maximum residual flow), respectively. Similarly as in the OC case, the condition leading to the strongest development of vorticity cores is the presence of a complete occlusion, for which the flow through the bypass starts creating a strong and complex vorticity pattern close to the heel. The minimum values of the three cost functionals are decreasing functions with respect to ω, an indication that the case $\omega = 0$ is the most difficult one concerning shape optimization (see Tab. 3); reduction in the cost functionals ranges from 24% to 70% for the different cases, compared to the reference domain case. The vorticity cores are clearly observable also in the optimal configuration in presence of a complete artery blockage; moreover,

https://doi.org/10.1051/m2an/2012059 Published online by Cambridge University Press

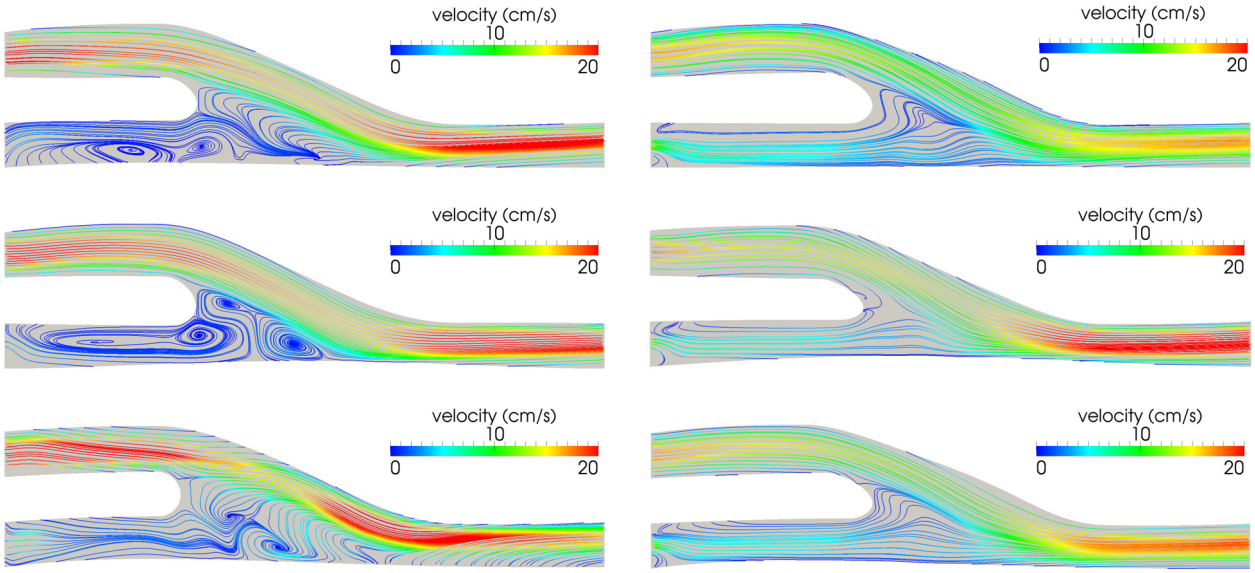


FIGURE 16. Optimal shapes in the cases $\omega = 0$ (left) and $\omega = \omega_{\max}$ (right) for the vorticity J_3, the Stokes tracking J_2 and the Galileian invariant J_4 functionals (from top to bottom).

TABLE 3. Results for shape optimization (DD-SO) in the cases $\omega = 0$ and $\omega = \omega_{\max}$ and robust shape optimization (RD-SO) problems.

	$\frac{J^*(\omega=0)}{J^*(\omega=\omega_{\max})}$	$\Delta J(\omega = 0\,,\ \omega = \omega_{\max})$	# I/O evals ($\omega = 0\,,\ \omega = \omega_{\max}$)	# I/O evals (robust)
J_3	1.257	26.3%, 24.2%	125, 27	389
J_2	1.924	63.2%, 55.3%	99, 64	416
J_4	1.267	65.4%, 70.7%	183, 63	973

although we obtain a clear reduction of vorticity also in this case, the vorticity cores never disappear completely. In the end, as for the OC case, we remark that the anastomosis angle decreases as the residual flow increases, since optimal shapes obtained in the case $\omega = \omega_{\max}$ (see Fig. 16) show a more elongated heel.

Concerning the solution of the robust design (RD-SO) problem, the robust configurations correspond to the optimal shapes computed for $\omega = 0$ in the previous case. In particular, the solution of the robust (shape) optimization problem requires about $\mathcal{O}(10^3)$ input/output evaluations, thus entailing a CPU time which is at least one order of magnitude larger than a (shape) optimization problem (see Tab. 3), ranging from $1 \div 4$ hours for the latter case to $13 \div 35$ hours for the former case. This indicates that a design that is robust over the entire range $\omega \in [0, \omega_{\max}]$ must be tuned mainly for the case of total occlusion.

7. CONCLUSION

We have reviewed the state-of-the art for optimal shape design of arterial bypass grafts. Using mathematical theory of optimal control and shape design, we have proposed two different worst-case optimization formulations to solve the problem of bypass design under uncertainty: (i) a boundary control formulation, which simplifies away the geometry and treats only the angle of the anastomosis as a boundary control variable, and (ii) a shape optimization formulation using a parametrized geometry to represent the anastomosis shape. We applied

https://doi.org/10.1051/m2an/2012059 Published online by Cambridge University Press

model reduction in the form of reduced basis methods to reduce the computational costs of solving the robust optimization problems in a preliminary 2D setting.

The literature on the design of bypass angles [37–41] proposes a variety of angles that have been suggested as optimal, ranging from 15–45° depending on the setting of the problem. Part of our motivation was to understand why such widely ranging "optimal" angles can be found. We have performed numerical tests on 2D steady flow cases to confirm the robustness of the obtained anastomosis angle with respect to the unknown residual incoming flow from the occluded artery. Five different cost functionals (energy dissipation, Stokes tracking, vorticity, Galilean-invariant vortex measure, wall shear stress gradient) taken from literature and proposed for the reduction of downstream vorticity were studied. The optimal anastomosis angle was found to depend strongly on the choice of the cost functional and on the flow split between the occluded branch and the bypass, but not very strongly on the particular shape of the flow profile. Our results are in line with those of [58]. We compared our 2D boundary control model against results obtained in a plane-symmetric 3D boundary control problem as well as a 2D shape optimization problem, where the toe shape could be directly optimized. Three dimensional effects were found not to have a large impact on the total downstream vorticity for moderate Reynolds numbers. Differences up to 10–20° in the optimal angle predictions were found between different cost functionals and flow split values used. In all cases studied the optimal angle increased as the severity of the occlusion in the host artery increased, which indicates that underestimating the level of occlusion in the host artery may lead to bypass designs with too small angles. Therefore, a robust bypass shape should be one that is tailored for the total occlusion of the host artery.

Acknowledgements. This work was partially funded by the European Research Council Advanced Grant "Mathcard, Mathematical Modelling and Simulation of the Cardiovascular System" (Project ERC-2008-AdG 227058), and by the Swiss National Science Foundation (Project 200021-122136). We acknowledge the use of the `rbMIT` package developed by the group of A.T. Patera (MIT) as a basis for the 2D reduced basis simulations (`http://augustine.mit.edu`). The 3D finite elements simulations presented in this paper have been computed using the open-source `LifeV` library (`http://www.lifev.org`). `LifeV` is a joint collaboration between four institutions: École Polytechnique Fédérale de Lausanne (CMCS) in Switzerland, Politecnico di Milano (MOX) in Italy, INRIA (REO, ESTIME) in France, and Emory University (Sc. Comp) in the USA.

References

[1] V. Agoshkov, A. Quarteroni and G. Rozza, A mathematical approach in the design of arterial bypass using unsteady Stokes equations. *J. Sci. Comput.* **28** (2006) 139–165.

[2] V. Agoshkov, A. Quarteroni and G. Rozza, Shape design in aorto-coronaric bypass anastomoses using perturbation theory. *SIAM J. Numer. Anal.* **44** (2006) 367–384.

[3] G. Allaire, *Conception optimale de structures*, vol. 58. Springer Verlag (2007).

[4] D. Amsallem, J. Cortial, K. Carlberg and C. Farhat, A method for interpolating on manifolds structural dynamics reduced-order models. *Int. J. Numer. Methods Eng.* **80** (2009) 1241–1258.

[5] H. Antil, M. Heinkenschloss, R.H.W. Hoppe and D.C. Sorensen, Domain decomposition and model reduction for the numerical solution of PDE constrained optimization problems with localized optimization variables. *Comput. Vis. Sci.* **13** (2010) 249–264.

[6] M. Berggren, Numerical solution of a flow-control problem: Vorticity reduction by dynamic boundary action. *SIAM J. Sci. Comput.* **19** (1998) 829.

[7] M. Bergmann and L. Cordier, Optimal control of the cylinder wake in the laminar regime by trust-region methods and POD reduced-order models. *J. Comput. Phys.* **227** (2008) 7813–7840.

[8] R.P. Brent, *Algorithms for Minimization Without Derivatives*. Prentice-Hall, Englewood Cliffs, N.J. (1973).

[9] E. Burman and M.A. Fernández, Continuous interior penalty finite element method for the time-dependent Navier–Stokes equations: space discretization and convergence. *Numer. Math.* **107** (2007) 39–77.

[10] K. Carlberg and C. Farhat, A low-cost, goal-oriented compact proper orthogonal decomposition basis for model reduction of static systems. *Int. J. Numer. Methods Eng.* **86** (2011) 381–402.

[11] T. F. Coleman and Y. Li, An interior trust region approach for nonlinear minimization subject to bounds. *SIAM J. Optim.* **6** (1996) 418–445.

[12] L. Dedè, Optimal flow control for Navier–Stokes equations: drag minimization. *Int. J. Numer. Methods Fluids* **55** (2007) 347–366.

[13] S. Dempe, *Foundations of bilevel programming*. Kluwer Academic Publishers, Dordrecht, The Netherlands (2002).

https://doi.org/10.1051/m2an/2012059 Published online by Cambridge University Press

[14] S. Deparis, Reduced basis error bound computation of parameter-dependent Navier-Stokes equations by the natural norm approach. *SIAM J. Numer. Anal.* **46** (2008) 2039–2067.
[15] S. Deparis and G. Rozza, Reduced basis method for multi-parameter-dependent steady Navier-Stokes equations: Applications to natural convection in a cavity. *J. Comput. Phys.* **228** (2009) 4359–4378.
[16] H. Do, A.A. Owida, W. Yang and Y.S. Morsi, Numerical simulation of the haemodynamics in end-to-side anastomoses. *Int. J. Numer. Methods Fluids* **67** (2011) 638–650.
[17] O. Dur, S.T. Coskun, K.O. Coskun, D. Frakes, L.B. Kara and K. Pekkan, Computer-aided patient-specific coronary artery graft design improvements using CFD coupled shape optimizer. *Cardiovasc. Eng. Tech.* (2011) 1–13.
[18] Z. El Zahab, E. Divo and A. Kassab, Minimisation of the wall shear stress gradients in bypass grafts anastomoses using meshless CFD and genetic algorithms optimisation. *Comput. Methods Biomech. Biomed. Eng.* **13** (2010) 35–47.
[19] C.R. Ethier, S. Prakash, D.A. Steinman, R.L. Leask, G.G. Couch and M. Ojha, Steady flow separation patterns in a 45 degree junction. *J. Fluid Mech.* **411** (2000) 1–38.
[20] C.R. Ethier, D.A. Steinman, X. Zhang, S.R. Karpik and M. Ojha, Flow waveform effects on end-to-side anastomotic flow patterns. *J. Biomech.* **31** (1998) 609–617.
[21] S. Giordana, S.J. Sherwin, J. Peiró, D.J. Doorly, J.S. Crane, K.E. Lee, N.J.W. Cheshire and C.G. Caro, Local and global geometric influence on steady flow in distal anastomoses of peripheral bypass grafts. *J. Biomech. Eng.* **127** (2005) 1087.
[22] M.D. Gunzburger, *Perspectives in Flow Control and Optimization. SIAM* (2003).
[23] M.D. Gunzburger, L. Hou and T.P. Svobodny, Boundary velocity control of incompressible flow with an application to viscous drag reduction. *SIAM J. Control Optim.* **30** (1992) 167.
[24] M.D. Gunzburger, H. Kim and S. Manservisi, On a shape control problem for the stationary Navier-Stokes equations. *ESAIM: M2AN* **34** (2000) 1233–1258.
[25] H. Haruguchi and S. Teraoka, Intimal hyperplasia and hemodynamic factors in arterial bypass and arteriovenous grafts: a review. *J. Artif. Organs* **6** (2003) 227–235.
[26] J. Haslinger and R.A.E. Mäkinen, *Introduction to shape optimization: theory, approximation, and computation. SIAM* (2003).
[27] R. Herzog and F. Schmidt, Weak lower semi-continuity of the optimal value function and applications to worst-case robust optimal control problems. *Optim.* **61** (2012) 685–697.
[28] M. Hintermüller, K. Kunisch, Y. Spasov and S. Volkwein, Dynamical systems-based optimal control of incompressible fluids. *Int. J. Numer. Methods Fluids* **46** (2004) 345–359.
[29] J.D. Humphrey, Review paper: Continuum biomechanics of soft biological tissues. *Proc. R. Soc. A* **459** (2003) 3–46.
[30] M. Jiang, R. Machiraju and D. Thompson, Detection and visualization of vortices, *in The Visualization Handbook*, edited by C.D. Hansen and C.R. Johnson (2005) 295–309.
[31] H. Kasumba and K. Kunisch, Shape design optimization for viscous flows in a channel with a bump and an obstacle, in *Proc. 15th Int. Conf. Methods Models Automation Robotics*, Miedzyzdroje, Poland (2010) 284–289.
[32] R.S. Keynton, M.M. Evancho, R.L. Sims, N.V. Rodway, A. Gobin and S.E. Rittgers, Intimal hyperplasia and wall shear in arterial bypass graft distal anastomoses: an in vivo model study. *J. Biomech. Eng.* **123** (2001) 464.
[33] D.N. Ku, D.P. Giddens, C.K. Zarins and S. Glagov, Pulsatile flow and atherosclerosis in the human carotid bifurcation. positive correlation between plaque location and low oscillating shear stress. *Arterioscler. Thromb. Vasc. Biol.* **5** (1985) 293–302.
[34] K. Kunisch and B. Vexler, Optimal vortex reduction for instationary flows based on translation invariant cost functionals. *SIAM J. Control Optim.* **46** (2007) 1368–1397.
[35] T. Lassila, A. Manzoni, A. Quarteroni and G. Rozza, *A reduced computational and geometrical framework for inverse problems in haemodynamics* (2011). Technical report MATHICSE 12.2011: Available on http://mathicse.epfl.ch/files/content/sites/mathicse/files/Mathicse
[36] T. Lassila and G. Rozza, Parametric free-form shape design with PDE models and reduced basis method. *Comput. Methods Appl. Mechods Eng.* **199** (2010) 1583–1592.
[37] M. Lei, J. Archie and C. Kleinstreuer, Computational design of a bypass graft that minimizes wall shear stress gradients in the region of the distal anastomosis. *J. Vasc. Surg.* **25** (1997) 637–646.
[38] A. Leuprecht, K. Perktold, M. Prosi, T. Berk, W. Trubel and H. Schima, Numerical study of hemodynamics and wall mechanics in distal end-to-side anastomoses of bypass grafts. *J. Biomech.* **35** (2002) 225–236.
[39] F. Loth, P.F. Fischer and H.S. Bassiouny. Blood flow in end-to-side anastomoses. *Annu. Rev. Fluid Mech.* **40** (200) 367–393.
[40] F. Loth, S.A. Jones, D.P. Giddens, H.S. Bassiouny, S. Glagov and C.K. Zarins. Measurements of velocity and wall shear stress inside a PTFE vascular graft model under steady flow conditions. *J. Biomech. Eng.* **119** (1997) 187.
[41] F. Loth, S.A. Jones, C.K. Zarins, D.P. Giddens, R.F. Nassar, S. Glagov and H.S. Bassiouny, Relative contribution of wall shear stress and injury in experimental intimal thickening at PTFE end-to-side arterial anastomoses. *J. Biomech. Eng.* **124** (2002) 44.
[42] A. Manzoni, *Reduced models for optimal control, shape optimization and inverse problems in haemodynamics*, *Ph.D. thesis*, École Polytechnique Fédérale de Lausanne (2012).
[43] A. Manzoni, A. Quarteroni and G. Rozza, Shape optimization for viscous flows by reduced basis methods and free-form deformation, *Internat. J. Numer. Methods Fluids* **70** (2012) 646–670.
[44] A. Manzoni, A. Quarteroni and G. Rozza, Model reduction techniques for fast blood flow simulation in parametrized geometries. *Int. J. Numer. Methods Biomed. Eng.* **28** (2012) 604–625.
[45] F. Migliavacca and G. Dubini, Computational modeling of vascular anastomoses. *Biomech. Model. Mechanobiol.* **3** (2005) 235–250.

https://doi.org/10.1051/m2an/2012059 Published online by Cambridge University Press

[46] I.B. Oliveira and A.T. Patera, Reduced-basis techniques for rapid reliable optimization of systems described by affinely parametrized coercive elliptic partial differential equations. *Optim. Eng.* **8** (2008) 43–65.

[47] A.A. Owida, H. Do and Y.S. Morsi, Numerical analysis of coronary artery bypass grafts: An over view. *Comput. Methods Programs Biomed.* (2012). DOI: 10.1016/j.cmpb.2011.12.005.

[48] J.S. Peterson, The reduced basis method for incompressible viscous flow calculations. *SIAM J. Sci. Stat. Comput.* **10** (1989) 777–786.

[49] M. Probst, M. Lülfesmann, M. Nicolai, H.M. Bücker, M. Behr and C.H. Bischof. Sensitivity of optimal shapes of artificial grafts with respect to flow parameters. *Comput. Methods Appl. Mech. Eng.* **199** (2010) 997–1005.

[50] A. Qiao and Y. Liu, Medical application oriented blood flow simulation. *Clinical Biomech.* **23** (2008) S130–S136.

[51] A. Quarteroni and G. Rozza, Optimal control and shape optimization of aorto-coronaric bypass anastomoses. *Math. Models Methods Appl. Sci.* **13** (2003) 1801–1823.

[52] A. Quarteroni and G. Rozza, Numerical solution of parametrized Navier-Stokes equations by reduced basis methods. *Numer. Methods Part. Differ. Equ.* **23** (2007) 923–948.

[53] A. Quarteroni, G. Rozza and A. Manzoni. Certified reduced basis approximation for parametrized partial differential equations in industrial applications. *J. Math. Ind.* 1 (2011).

[54] S.S. Ravindran, Reduced-order adaptive controllers for fluid flows using POD. *J. Sci. Comput.* **15** (2000) 457–478.

[55] A.M. Robertson, A. Sequeira and M.V. Kameneva, Hemorheology. *Hemodynamical Flows* (2008) 63–120.

[56] G. Rozza, On optimization, control and shape design of an arterial bypass. *Int. J. Numer. Methods Fluids* **47** (2005) 1411–1419.

[57] G. Rozza, D.B.P. Huynh and A.T. Patera, Reduced basis approximation and a posteriori error estimation for affinely parametrized elliptic coercive partial differential equations. *Arch. Comput. Methods Eng.* **15** (2008) 229–275.

[58] S. Sankaran and A.L. Marsden, The impact of uncertainty on shape optimization of idealized bypass graft models in unsteady flow. *Phys. Fluids* **22** (2010) 121902.

[59] O. Stein, *Bi-level strategies in semi-infinite programming.* Kluwer Academic Publishers, Dordrecht, The Netherlands (2003).

[60] R. Temam, *Navier-Stokes Equations.* AMS Chelsea, Providence, Rhode Island (2001).

[61] K. Veroy and A.T. Patera, Certified real-time solution of the parametrized steady incompressible Navier-Stokes equations: rigorous reduced-basis a posteriori error bounds. *Int. J. Numer. Methods Fluids* **47** (2005) 773–788.

[62] G. Weickum, M.S. Eldred and K. Maute, A multi-point reduced-order modeling approach of transient structural dynamics with application to robust design optimization. *Struct. Multidisc. Optim.* **38** (2009) 599–611.

[63] D. Zeng, Z. Ding, M.H. Friedman and C.R. Ethier, Effects of cardiac motion on right coronary artery hemodynamics. *Ann. Biomed. Eng.* **31** (2003) 420–429.

https://doi.org/10.1051/m2an/2012059 Published online by Cambridge University Press